The impact of Leaf Area Index on rainfall interception and the potential to estimate it using Sentinel-1 observations

TING DUAN
February, 2017

SUPERVISORS:
[Dr. Ir. R. van der Velde]
[Dr. Ir. C. van der Tol]

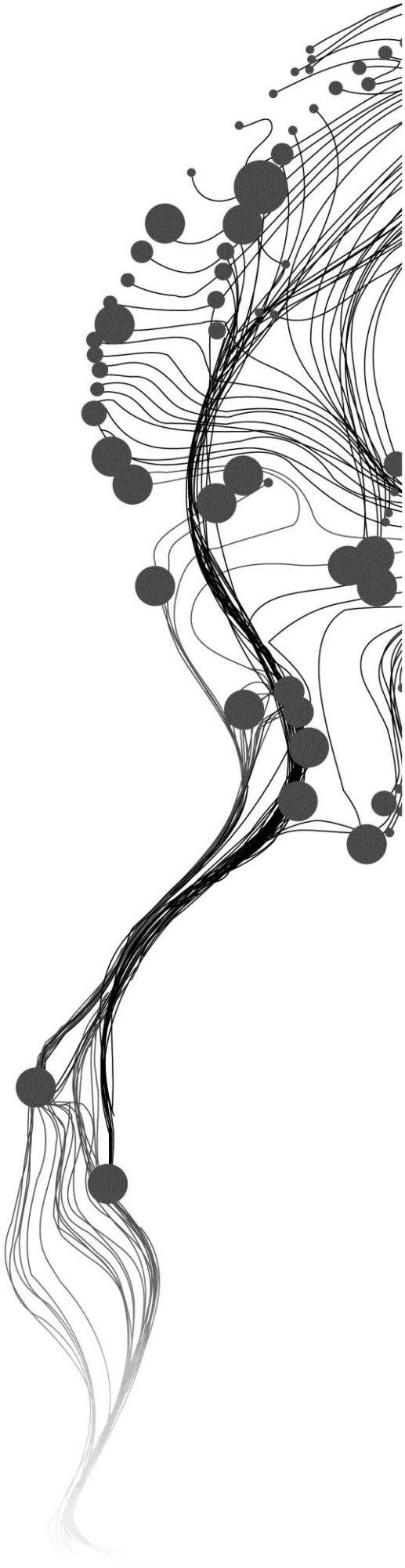

[The impact of Leaf Area Index on rainfall interception and the potential to estimate it using Sentinel-1 observations]

[TING DUAN]
Enschede, The Netherlands, [February, 2017]

Thesis submitted to the Faculty of Geo-Information Science and Earth Observation of the University of Twente in partial fulfilment of the requirements for the degree of Master of Science in Geo-information Science and Earth Observation.
Specialization: [Water Resources and Environmental Management]

SUPERVISORS:
[Dr. Ir. R. van der Velde]
[Dr. Ir. C. van der Tol]

THESIS ASSESSMENT BOARD:
[Dr. Ir. C.M.M. Mannaerts]
[Dr. D.C.M. Augustijn University of Twente]
etc

DISCLAIMER

This document describes work undertaken as part of a programme of study at the Faculty of Geo-Information Science and Earth Observation of the University of Twente. All views and opinions expressed therein remain the sole responsibility of the author, and do not necessarily represent those of the Faculty.

ABSTRACT

Rainfall interception accounts for a significant part of the water cycle in both forest and agricultural ecosystems. However, most researches focused on the forest interception and few focused on the crop interception. Corn as a typical seasonally dynamic crop can intercept a substantial amount of water at fully-grown stage. Knowing the amount of interception will improve hydrological models and enable water managers to make better informed decisions, for example regarding flood warnings.

In this study, rainfall, throughfall and vegetation parameters (including leaf area index (LAI), plant height) are measured once a week from May 2016 to November 2016 in the Twente region in the east of the Netherlands. The temporal and spatial variations of these parameters were analysed at field scale. The result showed that the interception of corn plants at its fully-grown stage can reach 90% of total rainfall. The rainfall interception is positively correlated with LAI.

The temporal and spatial variations of Synthetic Aperture Radar (SAR) Sentinel-1 C-band backscatter were also analysed at field scale. The correlation of the backscatter with LAI was investigated. However, the correlation of Sentinel-1 backscatter and LAI at field scale is low, R^2 is no more than 0.4. Sentinel-1 SAR images enable to monitor vegetation growth stage at a regional scale. Among the σ^0_{VH}, σ^0_{VV} and $\sigma^0_{VV}/\sigma^0_{VH}$ ratio, σ^0_{VH} is most sensitive to temporal variation of LAI at field scale. The polarization ratio has a lower sensivity to vegetation growth stage. σ^0_{VV} is also not very sensitive to vegetation growth stage, but it can be used together with σ^0_{VH} to distinguish vegetated and non-vegetated areas.

Very high interception ratios observed at corn fully-grown stage, it is so important to consider and monitor this component in agricultural areas. The interception is positively correlated with LAI, but it isn't available to estimate the interception using LAI. Sentinel-1 SAR images enable to monitor vegetation growth stage at a regional scale. But the correlation of Sentinel-1 backscatter and LAI is low, so it isn't possible for Sentinel-1 to estimate the exact value of LAI.

ACKNOWLEDGEMENTS

It was a very precious experience for the whole thesis research. I have gone to the field work for about three months, which was miserable at first but unforgettable at last. The working in corn fields make me recall the childhood playing with my cousin in a small village.
The author acknowledge the first supervisor Dr. Rogier van der Velde, second supervisor Dr. Christiaan van der Tol and Phd Harm-Jan Benninga for the direction and help during the whole research period. Some of the in-situ measurements and photos were taken by fieldwork group partner Yohannes Agide Dejen, also thanks him a lot. Finally show my acknowledge for my family and friends for support and comfort in this period.

TABLE OF CONTENTS

LIST OF FIGURES

LIST OF TABLES

1. INTRODUCTION

1.1. Background

During the rainfall process, some rainfall water directly falls onto the ground through the space between plants or temporally being stopped by the leaves and then drip off, which is called throughfall. However, other rain water either reaches the ground along the stem or trunk of the plants which is represented as stemflow or it is captured by the leaves and finally evaporates back to the atmosphere. The portion of rainfall being captured is defined as the interception (Crockford & Richardson, 2000). In general, the interception represents 11% to 22.8% of total gross rainfall in tropical and temperate forest areas and 8% to 18% in tropical agricultural lands,(Carlyle-Moses & Price, 1999; Cuartas et al., 2007; Jackson, 2000) which means that rainfall interception accounts for a significant part of the water cycle in both forest and agricultural ecosystems. Most research, however focused on the forest interception (Crockford & Richardson, 2000; Czikowsky & Fitzjarrald, 2009; Gerrits et al., 2010) and few(Frasson & Krajewski, 2013; Leuning et al., 1994) focused on the crop interception. Corn as a typical seasonally dynamic crop can intercept a substantial amount of water at fully-grown stage (Kozak et al., 2007). Knowing the amount of interception will improve hydrological models and enable water managers to make better informed decisions, for example regarding flood warnings.

In view of the importance of interception, many efforts have been made to quantify and model the process of rainfall interception. At first, studies(Merriam, 1960) used empirical relationships with gross rainfall. However, this method is very much dependent on the specific study site and plant type conditions. Later-on, models have been developed to improve on these site-dependencies. These models have proven to give more reliable interception estimates. Muzylo et al. (2009) gave a summary of the various types of rainfall interception models, that have been developed. Rutter et al. (1971) first developed a numerical interception model. This model is based on the running water balance of precipitation, throughfall, evaporation and canopy water storage change through time. However, the model is hindered for wide application because of the high data requirement. Gash (1979) developed an interception model based on the Rutter model but the numerical method was developed into an analytical method. This model is storm-based and uses daily rainfall as input. Assumptions are that there is only one storm event per day and the canopy has totally dried out before next rain event. Gash et al. (1995) further revised the original model to resolve the overestimation under sparsely vegetation conditions. Due to the simple physical principle and the few parameters, the Gash model is most widely used. It has been applied successfully for different forest species, e.g. deciduous broadleaved forest (Su et al., 2016), rain forest (Vernimmen et al., 2007) and shrubs (Liu Zhangwen et al., 2012) under different climate conditions, including semi-arid (Motahari et al., 2013), Mediterranean (Limousin et al., 2008) and tropical (Gomez-Peralta et al., 2008). Van Dijk and Bruijnzeel (2001a) further modified the revised Gash model to account for vegetation canopy that varies over time and achieved improved performances in seasonally dynamic vegetation species e.g. cassava, maize and rice and agricultural systems(Van Dijk and Bruijnzeel 2001b).In their model, Van Dijk and Bruijnzeel (2001a) induced Leaf Area Index (LAI) as a parameter to account for the vegetation dynamics and LAI was proved to have a strong influence on canopy interception.

Leaf cover is an important parameter controlling the interception ratio. Leaf Area Index (LAI) is defined as the maximum projected leaf area per unit ground surface (Myneni et al., 1997). It is a biophysical variable that highly correlates with interception and it is often used as an input for interception models. Many instruments are available for in-situ measurement of LAI, which include optical sensors such as the LAI-2000/2200 (Bauer et al., 2016; Pearse et al., 2016) and hemispherical photography (Brandão & Zonta, 2016; Woodgate et al., 2016). However, the drawbacks of in-situ measurement are that they are time consuming and difficult to apply across large spatial and temporal domains for monitoring purposes. Remote sensing is a method to capture spatial information efficiently. It provides an alternative to monitor LAI over large spatial domains. Satellites carrying optical sensors, such as Landsat, NOAA and IKONOs were successfully used for LAI estimation in many studies (Chen et al., 2002; Colombo et al., 2003; Friedl et al., 1994), but the main drawback is its dependence on sunlight and clear-sky conditions.

An alternative remote sensing technique is Synthetic Aperture Radar (SAR). The SAR antenna on board transmits microwave signal to the ground and receive the backscatter signals to form an image, which is the same as the working principle of Radar. For real aperture radar, high resolution is depending on narrow beam leading to long antenna. Sometimes it isn't available for the aircraft to carry a very long antenna because of the loading capacity and economic budget. SAR allows for the collection of microwave observation at high spatial resolutions with short antenna by utilizing the movement of aircraft and the time delay of backscattering signals.

SAR has been successfully applied in many agricultural researches, thanks to its sensitivity to crop growth and its working capabilities irrespective of cloud and day/night conditions. Baghdadi et al. (2009) analysed the potential of different SAR sensors to monitoring sugarcane crops and both cross-polarization (HV,VH) and co-polarization signal shown high correlation to the detection of crop harvest. Hosseini et al. (2015) tested the potential of SAR at C-band and L-band to estimate LAI of corn and soybean. The result showed higher correlation between dual-polarization (HH-HV or VV-HV) and LAI in C-band than that of in L-band for both corn and soybean fields. Jiao et al. (2011) reported that for corn fields, the cross polarization (HV) backscatter coefficient (σ^0) is highly correlated with LAI when LAI is under 3 m^2 m^{-2}. However the correlation between the σ^0 and LAI reduces at values greater than 3 m^2 m^{-2}, because of the signal saturation.

Copernicus, previously known as GMES (Global Monitoring for Environment and Security), is an earth observation programme by the European Space Agency (ESA) to provide environmental information continuously. A couple of satellite missions called Sentinel are developed to support the function of Copernicus programme. There are two sun-synchronous orbit satellites in Sentinel-1 mission which is the first mission in Copernicus programme. The first Sentinel-1 satellite which carries a C-band SAR sensor, was launched in 2014. The Sentinel-1 satellites provide VV and VH backscatter at a spatial resolution of 10m with a temporal resolution of four days over Europe. The Sentinel-1 shows improvement in spatial, temporal and radiometric resolution, revisit time and availability (Torres et al., 2012). Compared to the former SAR sensors by ESA, such as ERS-1 (European Remote Sensing), ENVISAT (Environmental Satellite), Sentinel-1 can also be an interesting candidate for LAI estimation.

To derive the LAI from SAR images, backscatter models were applied. Various radiative transfer models have been developed to simulate the backscatter from vegetation covered soils such as Water Cloud Model (WCM)(Attema & Ulaby, 1978) and more sophisticated single scatterer models(Bracaglia et al., 1995). The major difference between WCM and single scatterer models is that it based on rather simple

assumptions of scattering between vegetation structure and few parameters needed. Both methods have shown satisfactory results for different crop varieties. Lin et al. (2009) proposed a method to estimate LAI of sugarcane field in southern China from ASAR (ENVISAT Advanced SAR) dual-polarization HH/HV backscatter data. Bakare et al. (1997) investigated the promising potential of SAR data from ERS (1/2) to distinguish different grow stages of wet rice in Malaysia. Cookmartin et al. (2000) compared the performance of monitoring crop grow by SAR backscattering coefficient from ERS-1 and result calculated in a radiative transfer model in wheat, barley and oilseed rape fields.

In this study, the vegetation growth was monitored in the Twente regions for the period from May to October using in-situ measurements of LAI and crop height. Over the same period also rainfall and throughfall were measured in two corn fields using tipping buckets at one location per field and rain collectors at various locations. The Sentinel-1 data for these fields were retrieved to analyse the ability to distinguish the vegetation grow period and the correlation with LAI. Finally, backscatter maps at regional scale are produced to monitor the vegetation grow stage over time.

1.2. Problem definition

The interception of corn is hard to estimate because of the spatial and temporal variations throughout the field. The interception of corn in temperate climate hasn't been studied a lot yet. LAI as a vegetation variable is of vital importance to interception estimation. SAR data has already been successfully applied in LAI estimation. Sentinel-1 is a newly launched satellite carrying a C-band SAR sensor with good spatial and temporal resolution. The potential of Sentinel-1 SAR to estimate LAI hasn't been studied as well.

1.3. Research objective

The general objective of this research is to analyse the impact of vegetation to rainfall interception and the potential to monitor vegetation grow stage using Sentinel-1 SAR data.

To accomplish this, this research will study: (a) the variations at temporal and spatial scale of vegetation growth measurement; (b) the variations at temporal and spatial scale of rainfall and throughfall; (c) the variations at temporal and spatial scale of retrieved Sentinel-1 SAR backscatter coefficient; (d) the correlation between dual-polarization ratio ($\sigma^0_{VV}/\sigma^0_{VH}$) and LAI; (e) mapping of the backscatter coefficient at regional scale.

1.4. Research questions

The following research questions are formulated:

- Is the LAI a vegetation variable with which the rainfall interception can be estimated reliably?
- Can Sentinel-1 backscatter observation be used to detect different vegetation growth stages?
- How does the interception by vegetation vary spatially and temporally in year 2016?
- Is the Sentinel-1 dual-polarization ratio sensitive enough for quantifying the LAI?

1.5. Thesis outline

Section 1 is the introduction of this study, including the background, problem definition, objectives, and research questions. Section 2 introduces the basic information such as location, temperature etc. of the study area. Section 3 gives an description of the field measurements procedure of rainfall, throughfall and LAI. Section 4 offers the information about Sentinel-1 mission and the satellite data processing procedure. Section 5 and section 6 show the results and analysis of measurement and satellite backscatter data. Section 7 is the summary of the results and Section 8 gives some recommendations to the future study.

2. STUDY AREA

The study sites are located in the Twente region in the east of the Overijssel province in the Netherlands where the Faculty of ITC operates a regional scale soil moisture and temperature monitoring network (Dente, Vekerdy, Su, & Ucer, 2011). The twenty stations of the network are installed and continuously monitor soil moisture and soil temperature data over an area of 50 km * 40 km. The Netherlands is located in a temperate oceanic climate zone, with mild wet winters and mild wet summers. The average annual precipitation is around 760mm and rainfall is evenly spread over the year. The mean winter and summer temperatures are 3 ℃ and 17 ℃, respectively. The elevation varies from -3 to 50m above sea level. The land cover of the area is a mixture of agricultural fields, forests and urbanized regions. The dominant crop type cultivated in this region is corn.

Six fields near three soil moisture stations are selected for intensive field measurements where since May intensive field measurements of soil moisture and several vegetation variables (e.g. LAI, height) have been performed. At the sites, the measurements are performed at multiple fields where the corn is at different growth stages. The three focus stations are ITC-SM_10 (centered on 52.373278°N, 6.962278°E), ITC-SM_ 07(centered on 52.191040°N, 6.668272°E) and ITC-SM_02 (centered on 52.390833°N, 6.860111°E), shown in Figure 1. Table 1 shows the field size, land cover and soil type information of the fields adjacent to these soil moisture stations. The study to rainfall interception focuses on the corn fields.

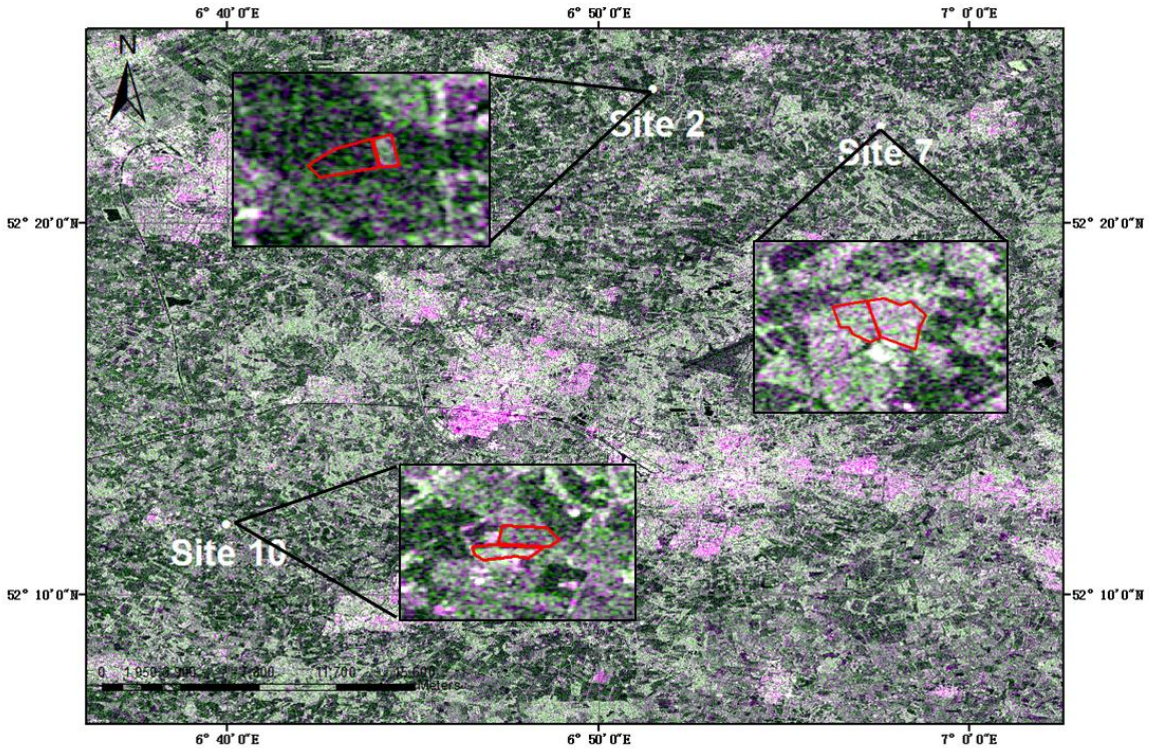

Figure 1 The location of study area (Sentinel-1 image on September 15, 2016. Band 1 power of $\sigma^0_{VV}/\sigma^0_{VH}$, Band 2 σ^0_{VH}, Band 3 σ^0_{VV})

Table 1 Basic information of study sites

Site number	**Field number**	**Field size (hectare)**	**Crop type**	**Soil type** (Wösten et al., 2013)	**Sow time (Day of year)**	**Harvest time (DOY)**
10	10-1	1.47	Corn	loamy soil with humus rich cover	152	283
	10-2	3.02	Potato	loamy soil with humus rich cover	146	-
7	7-1	4.45	Corn	loamy sand with a clay cover	209	320
	7-3	5.45	Corn	loamy sand with a clay cover	209	320
2	2-1	3.62	Grass	Man-made sandy thick earth soil	-	-
	2-2	1.28	Corn	Man-made sandy thick earth soil	166	274

3. FIELD MEASUREMENTS

Rainfall, throughfall, vegetation variables (including leaf area index, plant height) and soil moisture were measured from May 2016 to November 2016 at a nominal interval of a week to two weeks. To capture spatial variability and to estimate a reliable field average, there are five or six measurement locations within a single field. The locations are evenly distributed across the field. Figure 2 shows the fields and the white circles indicate the measurement locations. The dates, on which the measurements were collected, were selected correspond to the Sentinel-1 overpasses listed in Table 2.

Table 2 The dates of the measurements were collected ("√" indicates the measurement were taken in the specific field)

No.	Date	Field 10-1	Field 10-2	Field 7-1	Field 7-3	Field 2-1	Field 2-2
1	2016/05/25		√			√	
2	2016/06/06	√	√			√	
3	2016/06/23	√	√			√	√
4	2016/07/05	√	√			√	√
5	2016/08/10	√	√	√	√	√	√
6	2016/08/25	√	√	√	√	√	√
7	2016/09/06	√	√	√	√	√	√
8	2016/09/15	√	√	√	√	√	√
9	2016/09/22	√	√	√	√	√	√
10	2016/09/30	√	√	√	√	√	√
11	2016/10/07	√	√	√	√	√	
12	2016/10/14		√	√	√	√	
13	2016/10/19			√	√		
14	2016/10/28		√	√	√		
15	2016/11/03		√	√	√	√	
16	2016/11/11		√	√	√	√	

(a) (b) (c)

Figure 2 The study fields. (a) site 10, field 10-1, 10-2 (b) site 7, field 7-1, 7-3 (c) site 2, field 2-1, 2-2 (adapted from google earth)

3.1. Rainfall and throughfall

Rainfall and throughfall measurements were conducted at site 10 and site 7. We used Davis tipping bucket rain gauges (http://www.davisnet.com/product/rain-collector-with-flat-base-for-vantage-pro2/) for event-based rainfall monitoring, shown in figure 3a and figure 3b. The resolution of this rain gauge is 0.2 mm. The rain gauge is connected to a HOBO logger that automatically records the time of each tip.

The rainfall is being measured by a rain gauge installed at 1.2m height at the side of the fields in an open area, as shown in fig. 3a. Throughfall measurements were made using a tipping bucket installed at a 0.4 m height in the field in between two corn rows (fig. 3b). To verify the spatial variability of throughfall across the field, rain collectors are placed at three locations within two fields. At each location one rain collector was installed in the middle between two rows (same as Davis rain gauge) and one in the corn row (fig. 3c). Each rain collector is made of a plastic bottle with a funnel (diameter 11.5 cm) tied on the top of it. The water in the bottle is measured during each measurement day, once every week to two weeks.

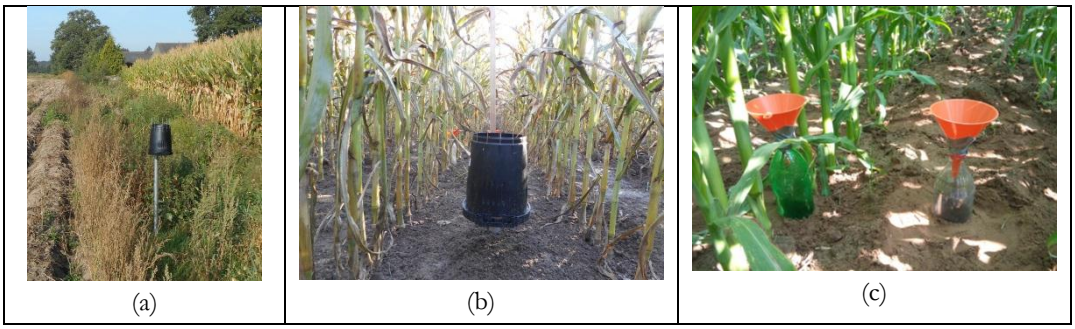

(a) (b) (c)

Figure 3 Photos of instrumentation used for rainfall and throughfall measurements, a) rain gauge installed at a height of 1.2 m at the side of ITC-SM_10, b) rain gauge installed at a height of 0.4 m in field 7-3 and c) two bottle rain collectors installed in and between corn rows in field 7-3 (photographs taken on 2016/09/30 (c) and 2016/11/11 (a and b)),.

3.2. Leaf Area Index

The leaf area index is measured by the LAI-2000 instrument (Li-Cor, Inc., Lincoln, Nebraska). A 270° viewing cap is used to prevent the influence of sun light and the operator on the sensor field of view. The measurements were all conducted under umbrella shadow or overcast conditions to block the sensor from direct sunlight and to reduce the light scattering effects.

For each measurement, the first reading was taken above the crop canopy and then four readings were taken under the canopy in between two corn rows (fig 4b). This measurement was performed two times at each location with the viewing direction in across and along corn row direction. When the corn reached 2 – 3 meters height, one reading is taken outside the field in the open air as the above canopy readings in the same field.

(a)

(b)

Figure 4: Photograph of the LAI measurement procedure; a) shows example of an independent LAI measurement, b) outlines the various measurement positions (photographs taken on 2016/11/11)

4. SENTINEL-1

4.1. Mission

Copernicus, previously known as GMES (Global Monitoring for Environment and Security), is an earth observation programme by the European Space Agency (ESA) to provide environmental information continuously. A couple of satellite missions called Sentinel from ESA cooperating with contributing missions from other space agencies and ground segment infrastructure are developed to support the function of Copernicus programme. The sentinel missions consist of Sentinel-1/2/3/4/5/5 Precursor/6 overall seven missions. Each mission has a platform of two satellites with the specific objective of earth observation.

Sentinel-1 ensures continuity of C-band (5.405 GHz centre frequency) SAR data acquisition by the ESA. Compared to previous SAR satellites missions by the ESA (ERS-1, ERS-2 and Envisat) and Canadian Space Agency (Radarsat-1, Radarsat-2), the Sentinel-1 mission aims at an improved revisit time, spatial coverage and reliability dataset. Table 3 shows the comparison between some popular C-band SAR satellites used to be or still active recently. The objectives of Sentinel-1 consist of monitoring sea ice zones and the arctic environment, surveillance of marine environment, monitoring land surface motion risks, mapping of land surfaces, mapping in support of humanitarian aid in crisis situations.

Figure 5 Artist view of a Sentinel-1 satellite in the orbit (taken from https://sentinel.esa.int/web/sentinel/user-guides/sentinel-1-sar/overview)

Table 3 Comparing C-band SAR satellite missions

Satellite mission	Launch date	Swath width	Spatial Resolution	Repeat cycle	Polarization
ERS-1	July 17, 1991	100km	25m	35 days	VV
ERS-2	April 21, 1995	960km	25m	35 days	VV
Radarsat-1	Nov.4, 1995	100km	30m	24 days	HH
Radarsat-2	Dec 14, 2007	100km	25m	24 days	full
Envisat	March 1,2002	110km	30m	35 days	HH,VV
Sentinel-1	April 3, 2014	250km	10m	12 days	HH-HV, VV-VH

4.2. Data specifications and availability

Sentinel-1 can acquire data in four different acquisition modes, which are Strip Map (SM), Interferometric Wide swath (IW), Extra Wide swath (EW) and Wave (WV) with varying swath widths and spatial resolutions. The SM Mode has 80 km swath and 5m x 5m spatial resolution. This mode operates at one of the six pre-defined elevation beams with a constant azimuth and elevation angle. This mode isn't used very often except for emergency conditions. The IW Mode has 250 km swath and 5m x 20m spatial resolution. The IW mode is most frequently used in the Sentinel-1 mission services which is also the primary operation mode for land monitoring. It is also used in this research. IW mode used Terrain Observation with Progressive Scans SAR (TOPSAR) technique to acquire data in three sub-swaths. Table 3 gives some additional information of IW mode. Extra-Wide-Swath Mode has 400 km swath and 20m x 40 m spatial resolution. It also applies TOPSAR technique but acquires data in five sub-swaths. EW mode mainly used in marine area for sea-ice monitoring. Wave Mode has 5m x 5 m spatial resolution, with alternating 23° and 36.5° incidence angles. It is the default working mode for open ocean area observation. All the data is freely available at Sentinels Scientific Data Hub (Copernicus programme) can be free access and download on the Internet. (From https://scihub.copernicus.eu/dhus/#/home)

Table 4 Technical information on IW mode

Mode	IW
Swath width	250km
Incidence angle	29.1°-46°
Looks	Multiple
Polarization	Dual HH-HV, VV-VH or Single HH,VV. Over land dual VV+VH.
Radiometric accuracy	1dB
Pixel spacing	10m * 10m

For this study, fifty-seven Sentinel-1 SAR images acquired in VH/VV dual polarization collected in the period from 1 May, 2016 to 27 October, 2016 were analysed. All the images are valid in IW mode as level-1 processed Ground Range Detected (GRD) product. Images in the GRD product has been ellipsoid projected to the ground. The Sentinel-1 overpass took place mainly at 17:15 (local time) or 5:40 (local time) in asending or descending overpass.

Table 5 List of Sentinel-1 SAR data sets of year 2016 used in this research

Index	Date (dd - mm)	Over pass time	Pass	Orbit	Index	Date (dd - mm)	Over pass time	Pass	Orbit
1	01-05	05:41	Descending	11061	30	17-08	05:41	Descending	12636
2	04-05	17:16	Ascending	11112	31	22-08	05:49	Descending	12709
3	06-05	05:49	Descending	11134	32	29-08	05:41	Descending	12811
4	09-05	17:24	Ascending	11185	33	01-09	17:16	Ascending	12862
5	13-05	05:41	Descending	11236	34	03-09	05:49	Descending	12884
6	16-05	17:16	Ascending	11287	35	06-09	17:24	Ascending	12935
7	18-05	05:49	Descending	11309	36	10-09	05:41	Descending	12986
8	21-05	17:24	Ascending	11360	37	13-09	17:16	Ascending	13037

9	25-05	05:41	Descending	11411	38	15-09	05:49	Descending	13059
10	28-05	17:16	Ascending	11462	39	18-09	17:24	Ascending	13110
11	30-05	05:49	Descending	11484	40	22-09	05:41	Descending	13161
12	02-06	17:24	Ascending	11535	41	25-09	17:16	Ascending	13212
13	06-06	05:41	Descending	11586	42	27-09	05:49	Descending	13234
14	09-06	17:16	Ascending	11637	43	30-09	17:24	Ascending	13285
15	11-06	05:49	Descending	11659	44	01-10	17:15	Ascending	2316
16	14-06	17:25	Ascending	11710	45	03-10	05:49	Descending	2338
17	30-06	05:41	Descending	11936	46	04-10	05:41	Descending	13336
18	05-07	05:49	Descending	12009	47	06-10	17:24	Ascending	2389
19	08-07	17:24	Ascending	12060	48	07-10	17:16	Ascending	13387
20	15-07	17:16	Ascending	12162	49	09-10	05:49	Descending	13409
21	17-07	05:49	Descending	12184	50	12-10	17:24	Ascending	13460
22	20-07	17:24	Ascending	12235	51	13-10	17:16	Ascending	2491
23	24-07	05:41	Descending	12286	52	15-10	05:49	Descending	2513
24	27-07	17:16	Ascending	12337	53	16-10	05:41	Descending	13511
25	01-08	17:24	Ascending	12410	54	18-10	17:24	Ascending	2564
26	05-08	05:41	Descending	12461	55	19-10	17:16	Ascending	13562
27	08-08	17:16	Ascending	12512	56	25-10	17:16	Ascending	2666
28	10-08	05:49	Descending	12534	57	27-10	05:49	Descending	2688
29	13-08	17:24	Ascending	12585					

4.3. Data pre- and post-processing

Figure 6 shows the whole procedure adopted for pre-processing for the downloaded Sentinel-1 GRD products. The Range Doppler Terrain Correction function in SNAP (Sentinel Application Platform software) is used to correct for image distortions caused by topography, but also performs the calibration and projection of images. Subsequently, the images are cut to the extent of the study area with the Subset function. These two operations are executed in software SNAP (http://step.esa.int/main/toolboxes/snap/). SNAP is developed by ESA for displaying and processing of Sentinel images.

The subsequent operations are executed in ENVI (Environment for Visualizing Images) and IDL (Interface Definition Language). Seamless Mosaic is used to mosaic two images that cover a part of the study area on the same date. Speckle noise in SAR images is caused by coherent sensing technique of multiple scatter distributed on the ground (Gagnon & Jouan, 1997). A speckle filter (median filter) with a 5*5 size window helps to reduce the noise. Then all the images are cut into exactly the same size. Finally the unit of σ^0 was converted from power ratio to dB (Decibel).

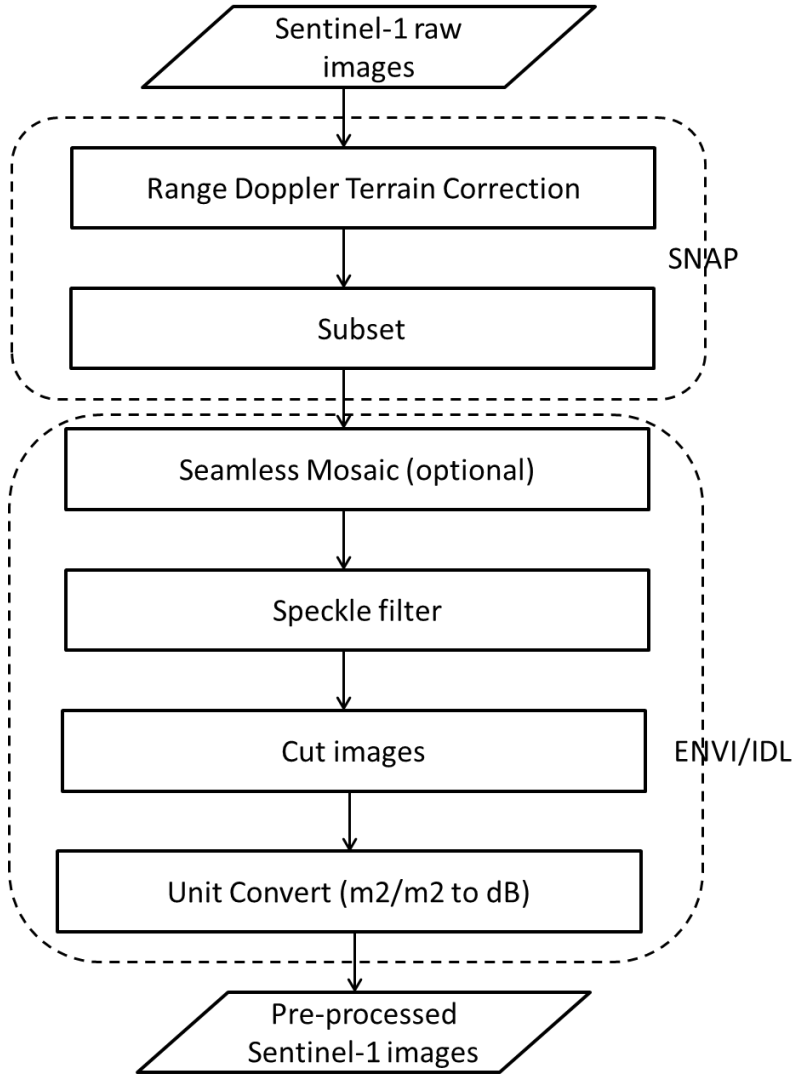

Figure 6 Flow chart of the Sentinel-1 SAR images pre-processing procedure

Figure 7 shows the procedure for the image post-processing. To better analyse the relationship between σ^0 and LAI, two methods are used for extracting the σ^0 value at field extent from the Sentinel-1 images. Firstly, the image was clipped to field extents using software ArcGIS. Then the σ^0 and incident angle are extracted and averaged using Matlab. Secondly, IDL was used to extract the 3 by 3 pixels plot size values and calculate an average backscatter around the measurement location.

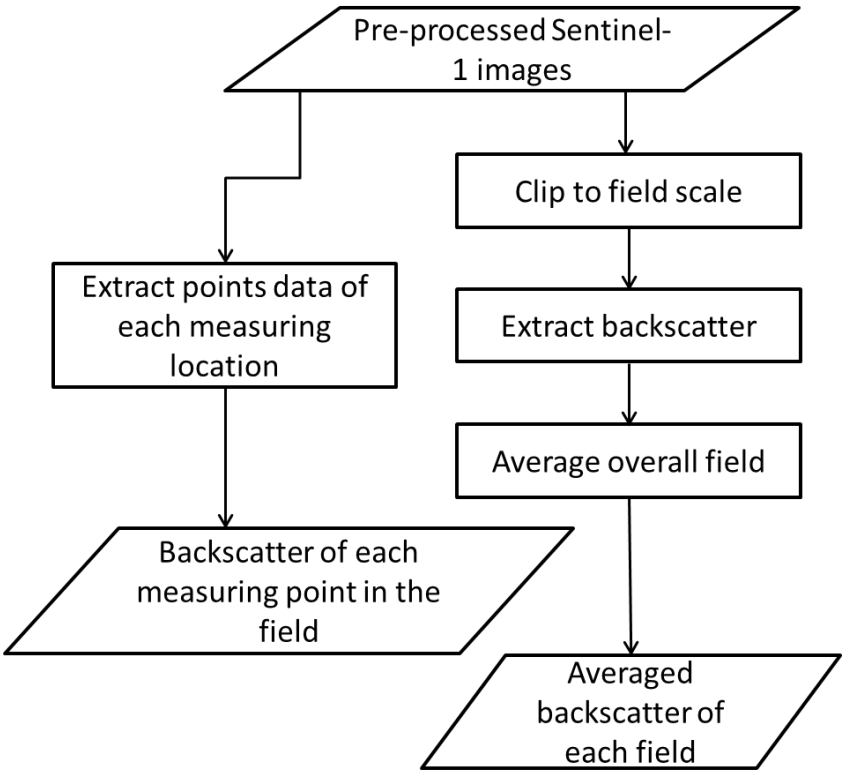

Figure 7 Flow chart of the Sentinel-1 SAR images post-processing procedure

5. MEASUREMENT ANALYSIS

5.1. Vegetation growth

5.1.1. Time series

Figure 8 shows the time series of vegetation variables, including vegetation height and LAI, measured in the field during the growing season. This is the average of the measurements from all locations within a field, considered as field average. The grow period of corn lasted for 4 months, about 120 days. Two distinct grow stages can be distinguished from figure 4a. The first stage is from the emergence until the plants reach the peak height, which takes about 50 days. The plants in fields 10-1 and 2-2 reached their peak heights at DOY 220 and in fields 7-1 and 7-3 at DOY 260. This is caused by the different sowing dates, which are DOY 152 and DOY 209 respectively. The peak plant heights vary from 240cm to 320cm. In the second stage, the plants stopped growing in height.

In figure 4b, the time series of LAI show three stages; growth, peak biomass and senescence. From emergence to the full biomass, the LAI increases corresponding to the trend in plant height (see figure 4a). This stage takes about 50 days. In field 10-1, the peak value occurred on DOY 220, which is the earliest time of plants reaching maximum height. Then the LAI remains at the same level for 30-40 days. After that plants wilt, the leaves turned yellow and the LAI decreased. In field 10-2, the peak value occurred on DOY 250. Then the LAI remains at the same level for about 40 days. After that part of the potato field is harvested so the LAI decreased (see figure 4c). The grass in field 2-1 is mowed regularly; the LAI reached peak value on DOY 187 then dropped to the lowest value on DOY 238, which can be inferred that time interval between two mow operations is about three months.

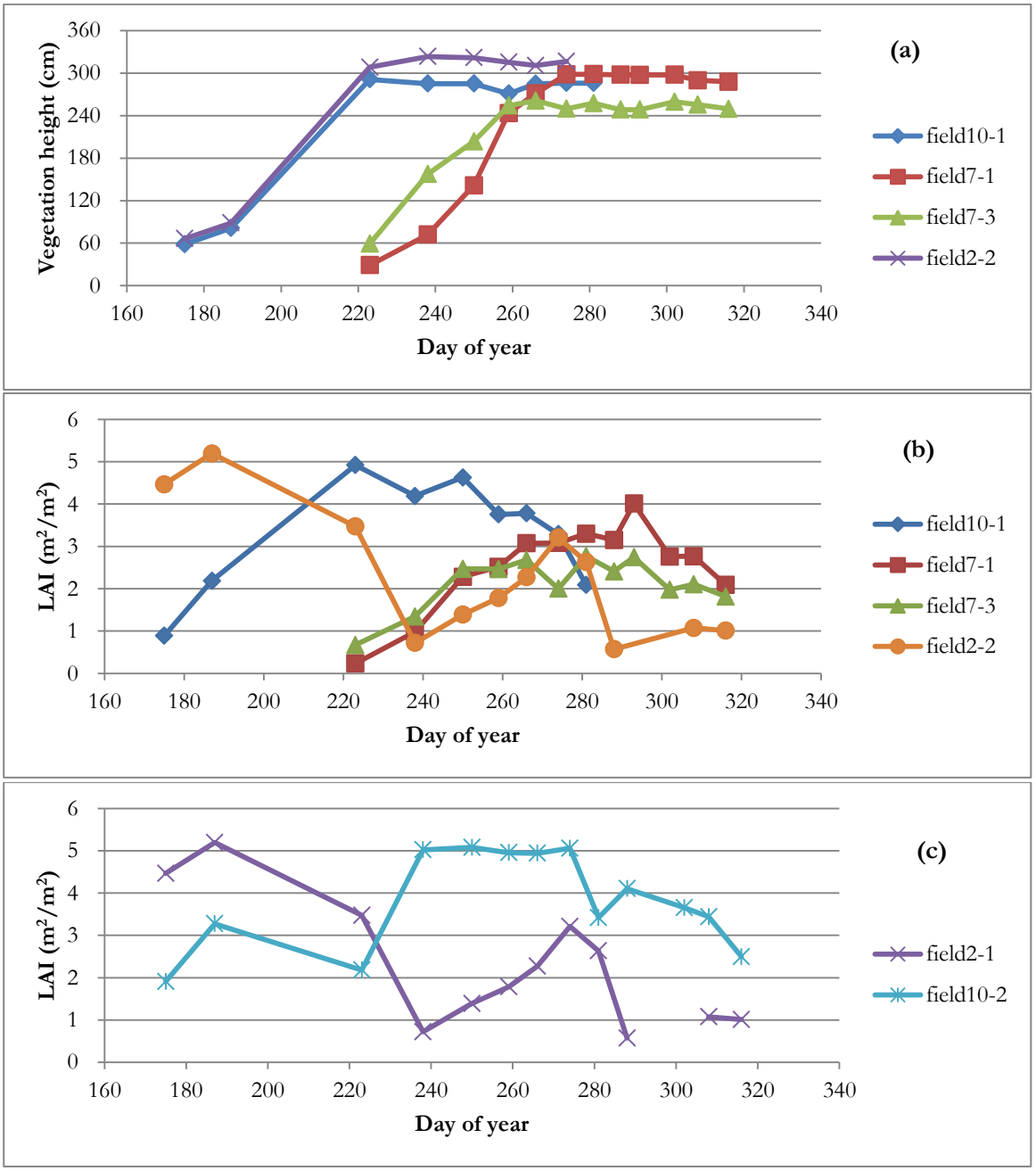

Figure 8 Temporal variations in field-averaged measurements of vegetation variables (LAI, plant height) (a) vegetation height measured in four corn fields; (b) LAI measured in four corn fields; (c) LAI measured in potato and grass fields.

5.1.2. Spatial distribution

The spatial variations of LAI and vegetation heights for all fields are presented in figures 9 and 10. The average value and standard deviation (std) of all the measurements during the crop grow season were calculated for each measuring position. The measurement positions corresponds to the position numbers are indicated in Figure 2.

For corn field 10-1, location 1 has the highest height as 250.31 cm. The height in location 3 is the lowest with 215.7 cm. Regarding the LAI, location 4 has the highest LAI with 3.54 m²/ m². The LAI in location 5

is the lowest with 2.85 m^2/ m^2. The difference between the highest and lowest value of vegetation height and LAI are respectively 34.61 cm and 0.69 m^2/ m^2. The std of height is highest in location 4 and lowest in location 3. The std of LAI is highest in location 3 and lowest in location 1. The low height in location 3 may because of weeds there absorbed the nutrient in the soil. So the corn plant is restricted of growing up.

For corn field 7-1, location 3 has the highest height with 245.64 cm. The height in location 1 is the lowest with 224cm. Considered with the LAI, location 3 has the highest LAI with 2.64. The LAI in location 1 is the lowest with 2.23. The difference between highest and lowest value of vegetation height and LAI are respectively 21.64 cm and 0.41 m^2/ m^2. The std of height is highest in location 3 and lowest in location 2. The std of LAI is highest in location 3 and lowest in location 1. During the in-situ measurement, the growth condition of plants around location 1 is worse than other locations, which match with the result of height and LAI.

For corn field 7-3, location 5 has the highest height with 236.53 cm. The height in location 1 is the lowest with 202.53 cm. Considered with the LAI, location 1 has the highest LAI with 2.23 m^2/ m^2. The LAI in location 6 is the lowest with 1.67 m^2/ m^2. The difference between highest and lowest value of vegetation height and LAI are respectively 34cm and 0.56 m^2/ m^2. The std of height is highest in location 5 and lowest in location 1. The std of LAI is highest in location 1 and lowest in location 6. During the in-situ measurement, the plants around location 1 were also not in very good growth condition, which match with the result of height.

For corn field 2-2, location 3 has the highest height with 258.48 cm. The height in location 1 is the lowest with 254.53 cm. Considered with the LAI, location 2 has the highest LAI with 3.21 m^2/ m^2. The LAI in location 1 is the lowest with 3.02 m^2/ m^2. The difference between highest and lowest value of vegetation height and LAI are respectively 3cm and 0.19 m^2/ m^2. The std of height is highest in location 1 and lowest in location 2. The std of LAI is highest in location 1 and lowest in location 3. The spatial variation in this field is relatively small, this may because the field size is not very large and the soil condition is homogenous throughout the field.

For grass field 2-1, location 2 has the highest height with 21.67 cm. The height in location 1 is the lowest with 20.46 cm. Considered with the LAI, location 1 has the highest LAI with 2.42 m^2/ m^2. The LAI in location 4 is the lowest with 2.22 m^2/ m^2. The difference between highest and lowest value of vegetation height and LAI are respectively 1.21 cm and 0.2 m^2/ m^2. The std of height is highest in location 3 and lowest in location 2. The std of LAI is highest in location 1 and lowest in location 5.

For potato field 10-2, location 5 has the highest LAI with 4.71 m^2/ m^2. The LAI in location 6 is the lowest with 3.47 m^2/ m^2. The difference between highest and lowest value of LAI is 1.24 m^2/ m^2. The std of LAI is highest in location 5 and lowest in location 6.

Among the four corn fields, field 2-2 has the highest plant height. Field 10-1 has the highest spatial variation of vegetation height and LAI. The vegetation height and LAI has a strong positive relationship, the locations with high vegetation height typically also have a high LAI values.

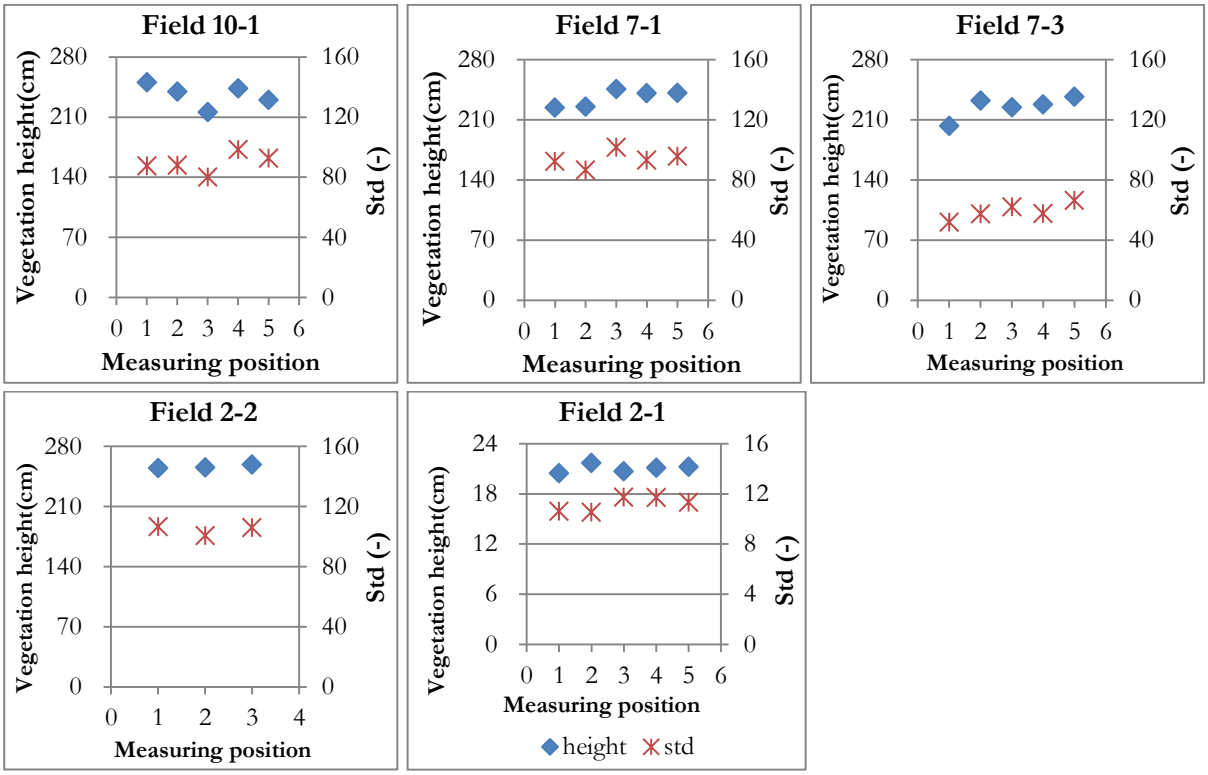

Figure 9 Spatial variations in location-averaged measurements of vegetation height, the standard deviation is shown in right y axis (field number is indicated at the top of the image).

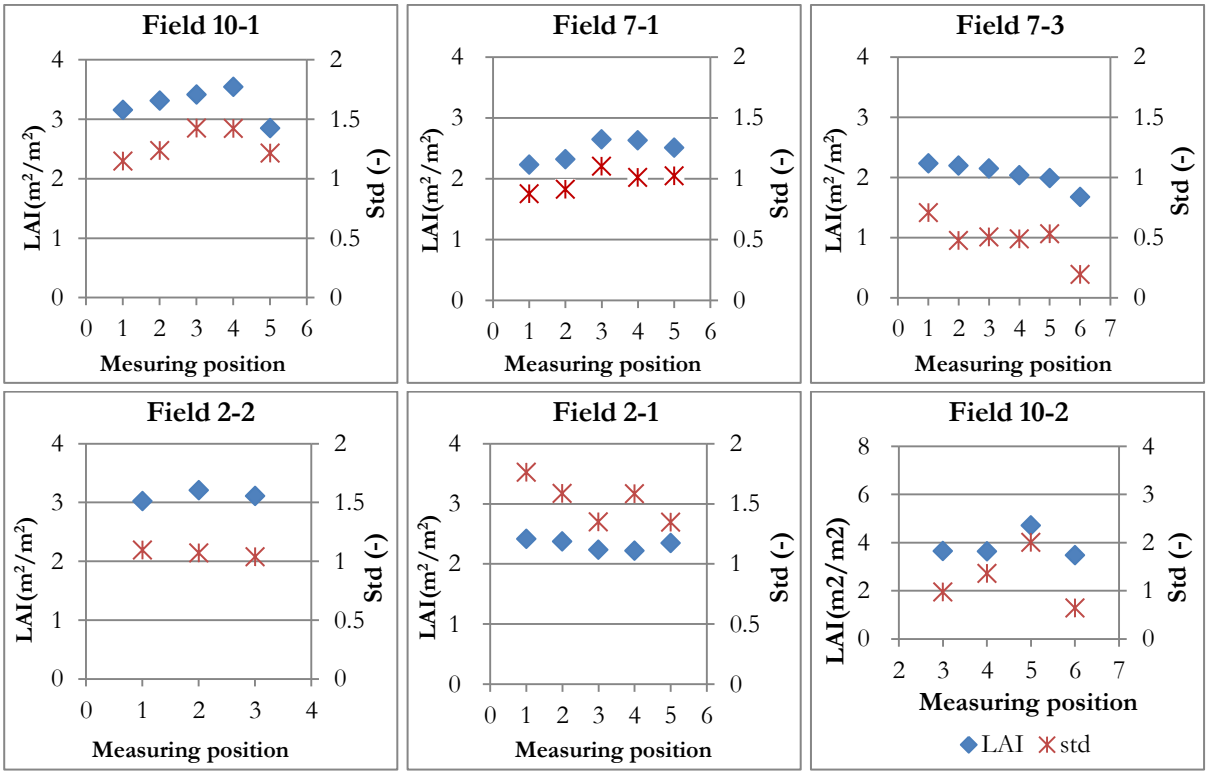

Figure 10 Spatial variations in location-averaged measurements of LAI, the standard deviation is shown in right y axis (field number is indicated at the top of the image).

5.2. Rainfall and throughfall

5.2.1. Time series

Figure 11 shows the time series of the ratio of the throughfall over rainfall measured by the rain gauges installed inside and outside of fields 10-1 and 7-3 (see chapter 3). The right vertical axis shows the LAI. The rainfall and throughfall data have been aggregated to a single day time. Under vegetated circumstances, the ratio should be equal to or less than 1. However, at the early growth stages, the ratio is higher than 1. This may be caused by rain drops splashed from the ground and also the wind effect and the leaves might be orientated and drip water into the bucket.

For field 10-1, the highest ratio (1.14) occured on DOY 176. Then the ratio decreases as the corn plants grow, since less water can go through the canopy and reaches the ground. On DOY 232, the ratio is as low as 0.1 for a crop height of around 2.85 m. While the plants are fully grown, the ratio remains at a low level around 0.1 - 0.2. After that, the ratio increases slightly. This is because while the plants were in senescence stage, the leaves wilted and let more water going through the canopy.

For field 7-3, the highest ratio happened on DOY 226 as 1.5. Then the ratio decreases as the corn plants grow. On DOY 302, the ratio is the lowest as 0.12.While the plants are fully grown, the ratio kept stable at a low level around 0.3 - 0.5. The interception of field 10-1 at fully grown stage is higher than that in field 7-3. The LAI of fields 10-1 is also higher than that in field 7-3 at fully grown stage.

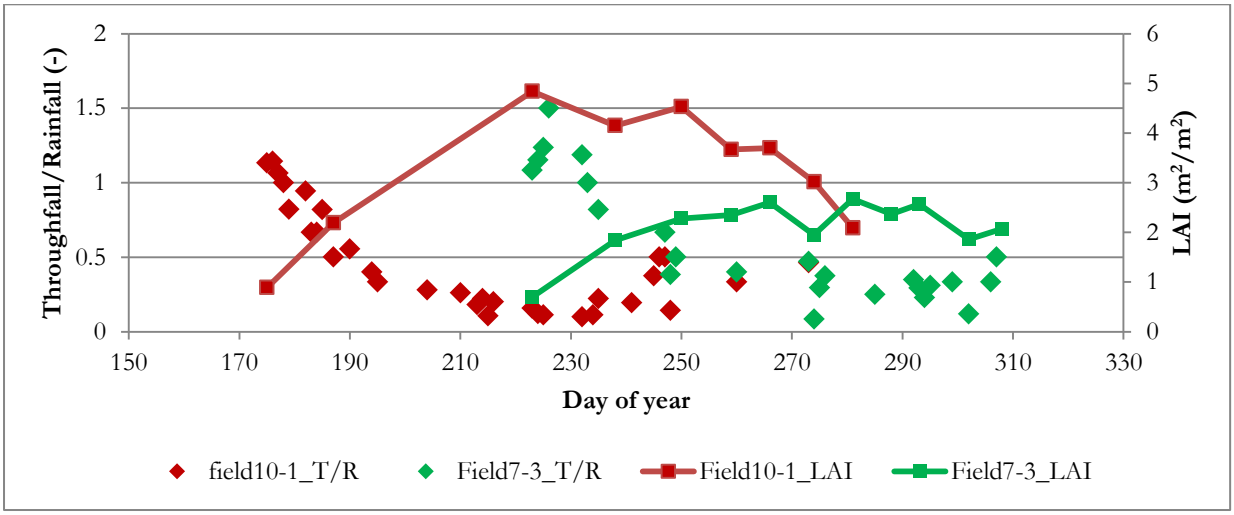

Figure 11 The temporal variation of throughfall over rainfall ratio obtained from rain gauge installed in fields 10-1 and 7-3, LAI measurements are also shown as a comparision.

5.2.2. Spatial variability

In Figure 12, the throughfall/rainfall ratio which is measured by bottle rain collectors is plotted for each location in the fields. The average value and standard deviation of all the measurements during the crop grow season for each measuring position were calculated. The field names are shown above the images. The throughfall/rainfall ratio is calculated based on the accumulation between two visiting dates divided by the measured rainfall with the tipping bucket outside the field. The location averaged LAI is plotted on the right vertical axis.

For field 7-1, location 1 has the highest average ratio as 0.61 and location 3 has the lowest value as 0.43. Location 3 has the highest average LAI value as 2.64 and location 1 has the lowest LAI value as 2.23, which is a perfect corresponding that the vegetation in location 1 is not as high as other locations especially location 3. For field 7-3, location 1 has the highest average ratio as 0.77 and location 4 has the lowest value as 0.28. Location 1 has the highest average LAI value as 2.23 and location 6 has the lowest LAI value as 1.67 which doesn't correspond well to the throughfall/rainfall ratio. The vegetation in location 1 is high but the ratio is also high.

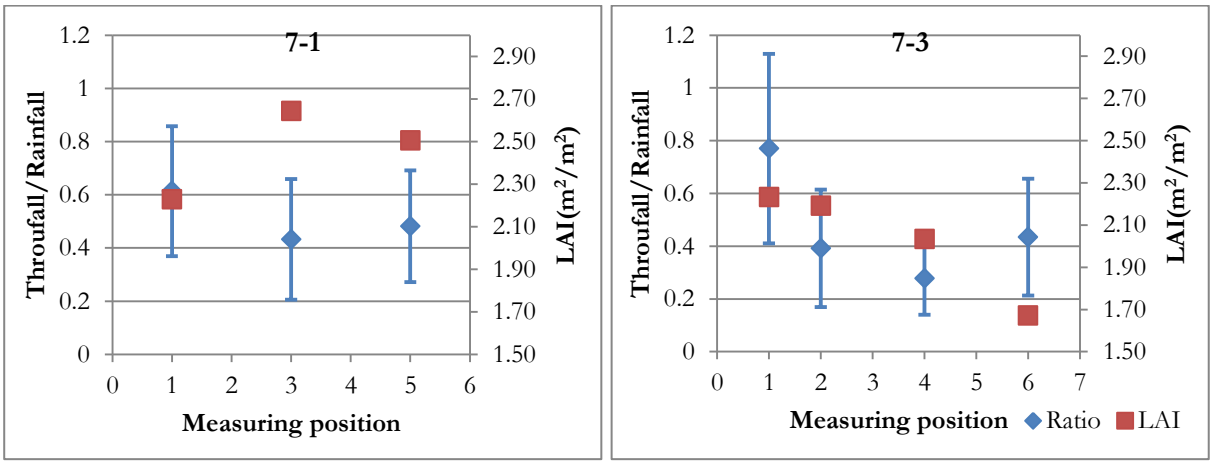

Figure 12 Spatial variability of throughfall/rainfall measured by bottle rain collectors (The standard deviation is plotted positively and negatively by the average data)

The average throughfall over rainfall ratio of all the bottle collectors in fields 7-1 and 7-3, the value of bottle collector installed near the rain gauge in field 7-3 and the ratio of rain gauge installed in field 7-3 are plotted in Figure 13a. The difference between ratio calculated from bottle collector near the rain gauge and the rain gauge is rather big except for the time period around DOY 293 and 302. Sometime the bottle measurements are much higher than the rain gauge, other times not. This may because of the random orientation of corn leaves and drip the water into the bottles or the rain gauge. The results for average of all the bottles and the rain gauge are rather close to each other. The difference is always smaller than the difference between bottles near the rain gauge and rain gauge except for the period around DOY 308 and 316. This may because that the average data reduce the effect of random orientation of corn.

For Figure 13b, the throughfall collected by the bottles installed between the corn rows is always much higher than the bottles installed in the corn rows. Considering the in-situ condition, the space above the bottles between the rows is more than the ones in the row, so more water is let in to the bottle. However, the results in the rows perfectly match with the rain gauge measurements, with the difference no more than 0.2. So this result may lead to the conclusion that bottle throughfall measurements in the row are more reliable than bottle measurements between the rows.

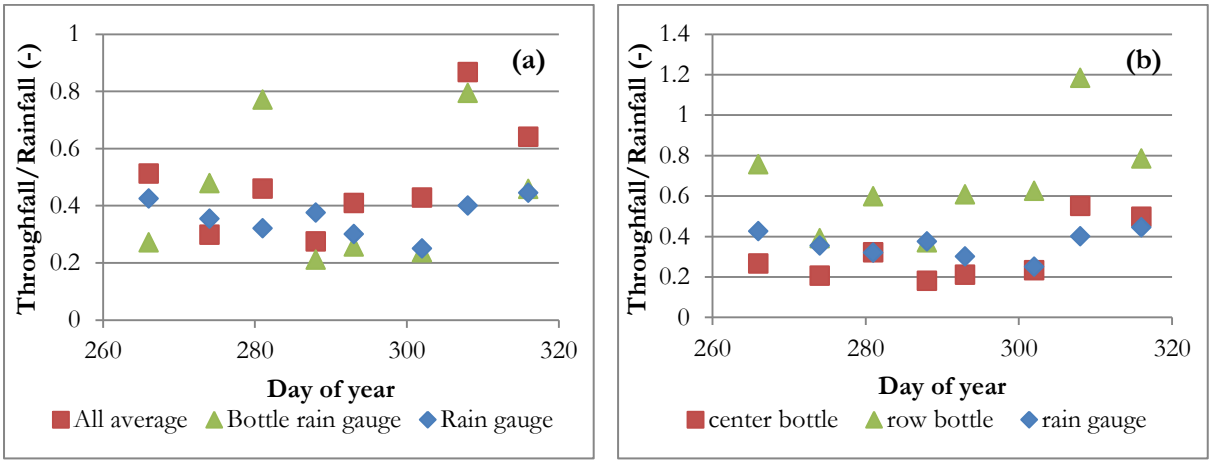

Figure 13 The variation of throughfall/rainfall measurements for bottle collectors and rain gauge. (a) throughfall /ratio calculated from average of bottles from all the locations, bottles near the rain gauge and the rain gauge respectively; (b) throughfall /ratio calculated from average of bottles in and between corn rows and the rain gauge respectively

6. SATELLITE DATA ANALYSIS

6.1. Backscatter coefficient

6.1.1. Time series

Figure 14 - 16 illustrate the time series of the backscatter coefficient at VV, VH and dual polarization ratio (VV/VH) using the equation $\sigma^0_{VV} - \sigma^0_{VH}$ when the unit is dB averaged over the fields. The horizontal axis represents time as the day of year. The left vertical axis is the average value of VV, VH and dual polarization ratio over the fields. The right vertical axis is the average of LAI measurement values over the field as a reference. The four corn fields (field 10-1, 7-1, 7-3 and 2-2) seem to have very similar performance, so only field 10-1 is shown and the images of other corn fields are given in the Appendix. Overall, Sentinel-1 has very good performance in showing the temporal variation of vegetation grow stage especially for corn and potatoes. The acquirision of all the satellite images are in the nominal incidence angles of 35°and 44°. The difference between two incidence angles is not very large.

Corn fields

Figure 14 shows the backscatter coefficients for the corn field 10-1. The VH in this corn field started to increase from DOY 160 to 190. During this period, the corn plants kept growing and the LAI increased. From DOY 190 to 240, the VH keeps approximately constant. During this period the corn stopped growing in height and started flowering and fruiting. After that, both LAI and VH decreased. The VV shows similar global trend as VH, except that the value difference between the two incidence angles is larger than for the VH channel. The polarization ratio started to decrease from DOY 160 to 190. During this period, the corn plants kept growing and the LAI also increased. The complexity of vegetation canopy increased so that the VV/VH ratio decreased. From DOY 190 to 240, the ratio stayed at approximately the same level. After that the ratio increased as the LAI decreased.

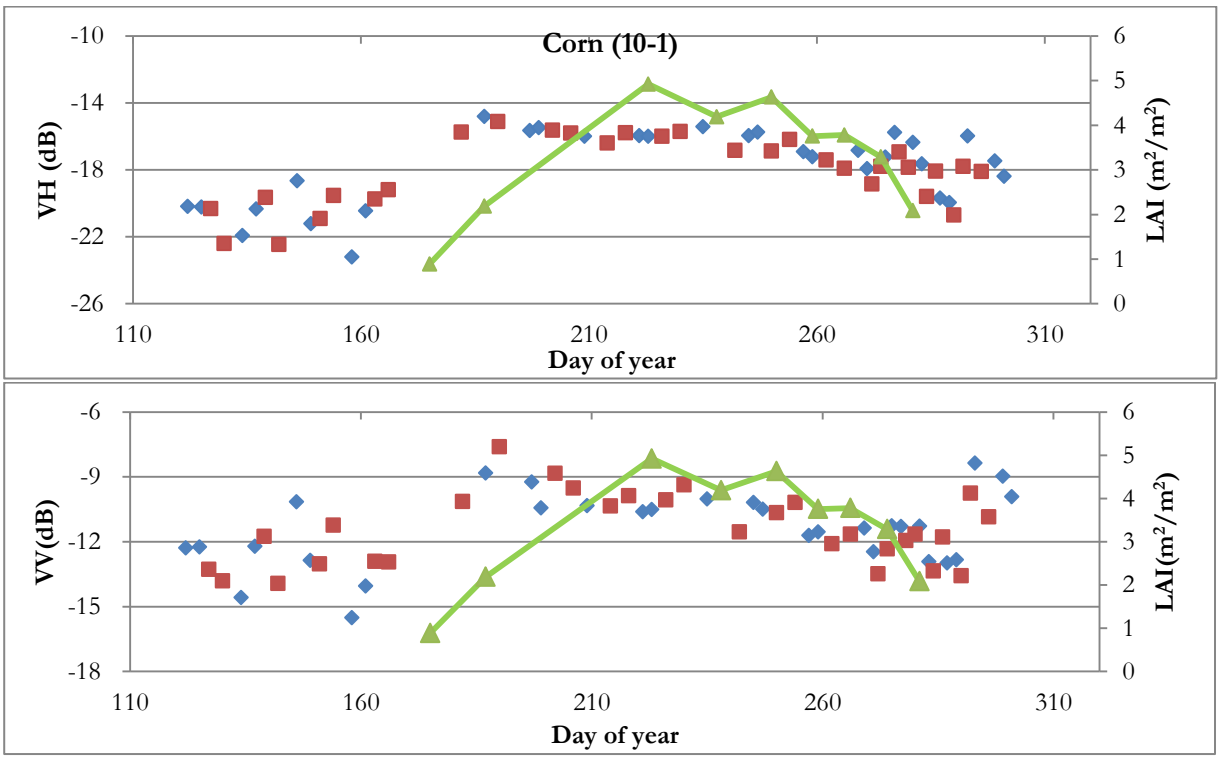

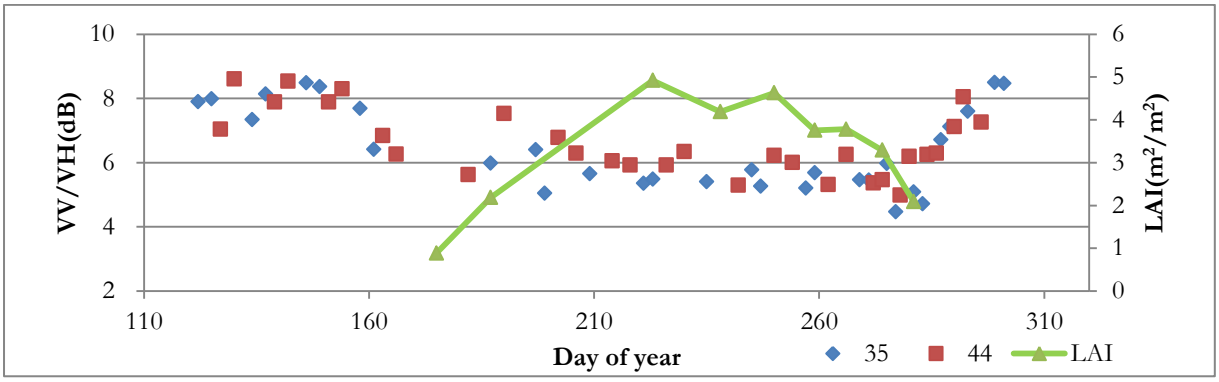

Figure 14 Time series of Sentinel-1 SAR backscatter coefficient in corn field (number 35, 44 means different incidence angles)

Potato field

Figure 15 shows the average backscatter coefficient in the potato field 10-2. The time period of VH increase in potato field is almost the same as that in the corn field. From DOY 190 to 220, the VH stayed at approximately the same level and didn't change too much. During this period the potato stopped growing in height and started fruiting. After that the VH decreased however the LAI didn't decrease. This performance is caused by the whole potato field was divided in three parts with different plant time. At that time, some of the potatoes were already harvested. The VV shows almost the same global trend as VH. The polarization ratio started to decrease from DOY 160 to 190. During this period, the potato plants kept growing and the LAI also increased. The complexity of vegetation canopy increased so that the VV/VH ratio decreased. From DOY 190 until the end of the period, the ratio stayed at approximately the same level.

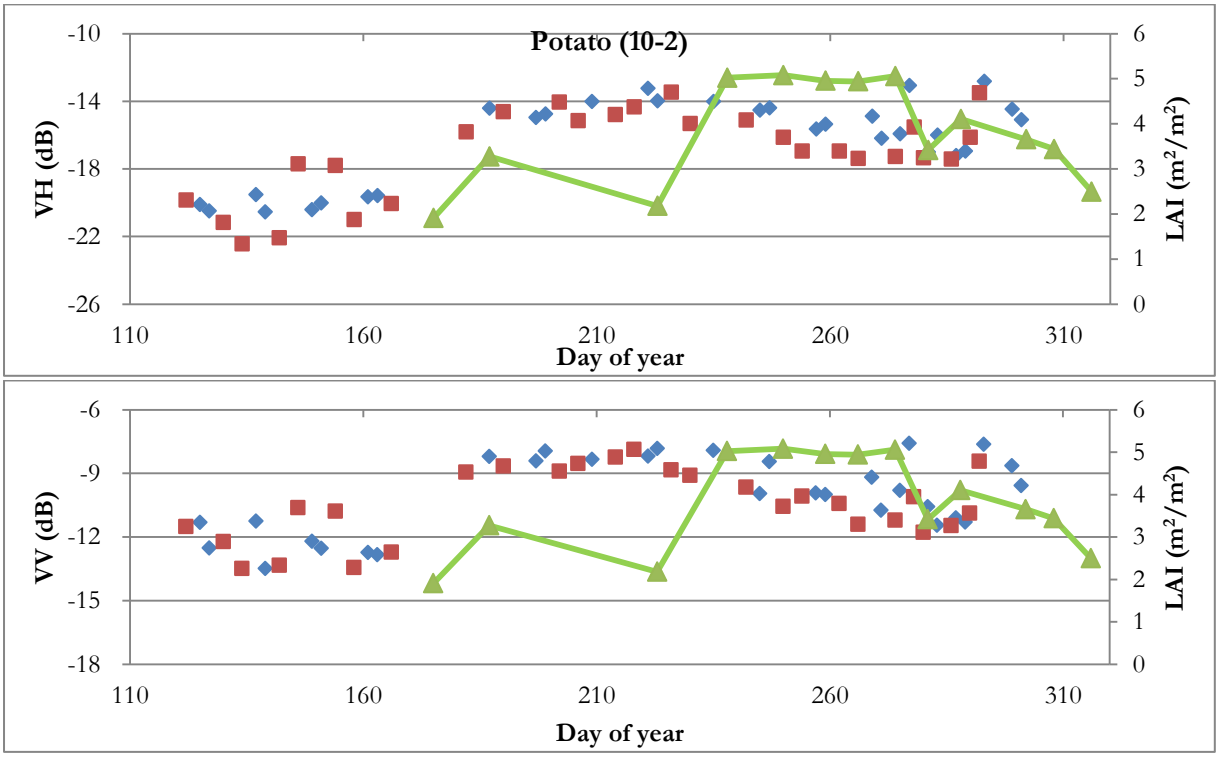

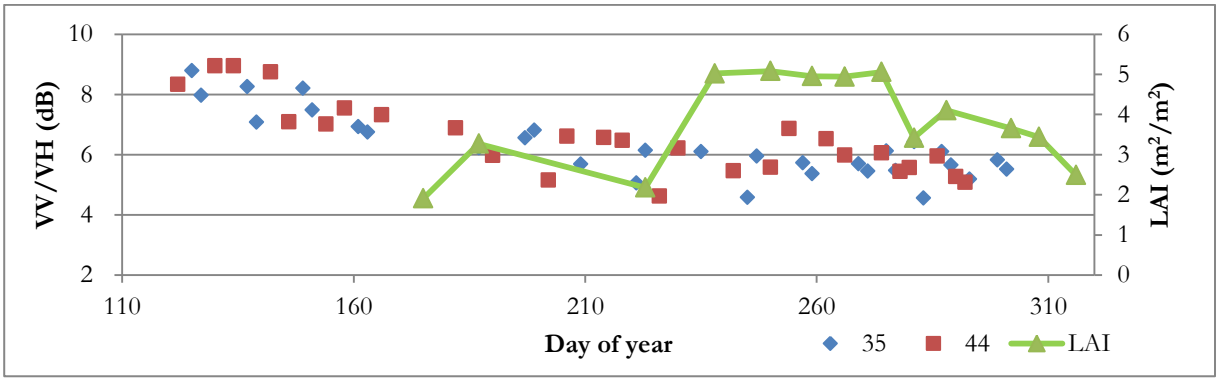

Figure 15 Time series of Sentinel-1 SAR backscatter coefficient in potato field (number 35, 44 means different incidence angles

Grass pasture

Figure 16 shows the backscatter coefficient in the grass field 2-1. The development of grass fields is different from other crops. The grass is mowed regularly. There are two mowed cycles during this period. The LAI reached the high peak at DOY 154. Then the VH decreased immediately because of cutting the grass. After that the VH increased gradually until being mowed again around DOY 238 and 288. The VV shows almost the same global trend as VH. The temporal variation of polarization ratio is not very obvious. This may because of the difficulties in precise grass LAI measurement and the vegetation type.

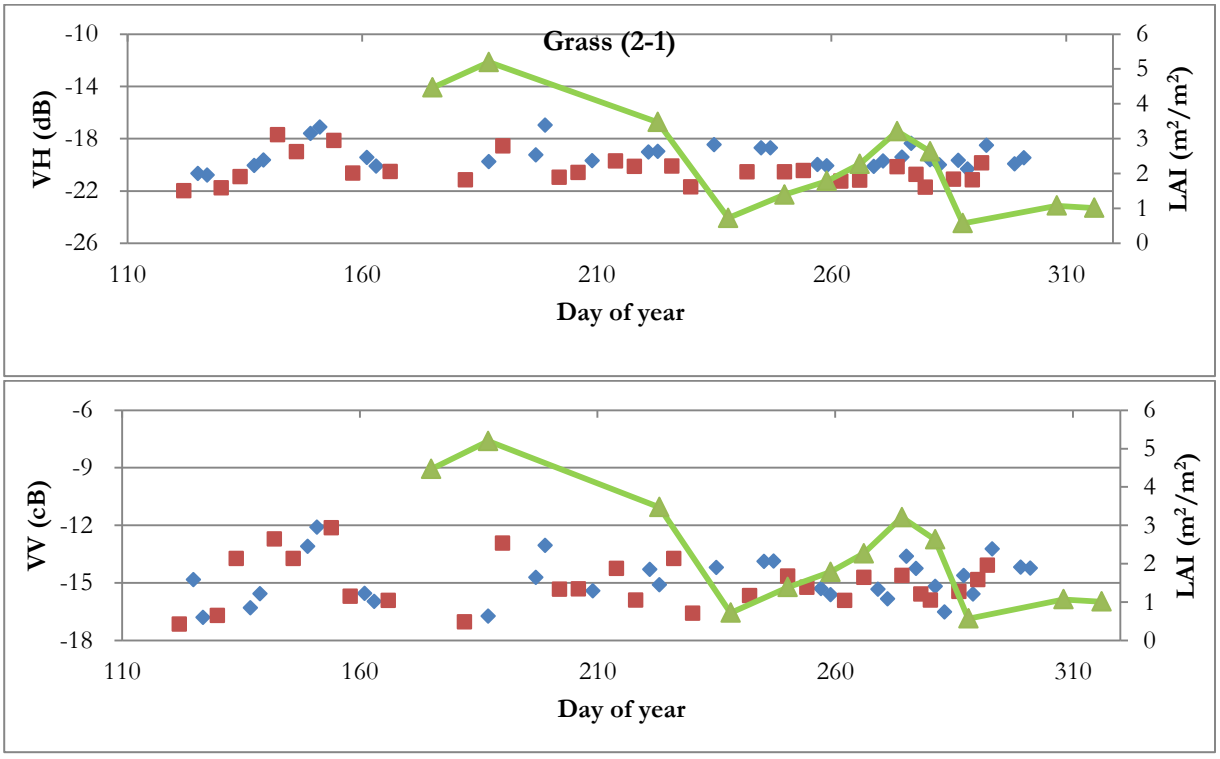

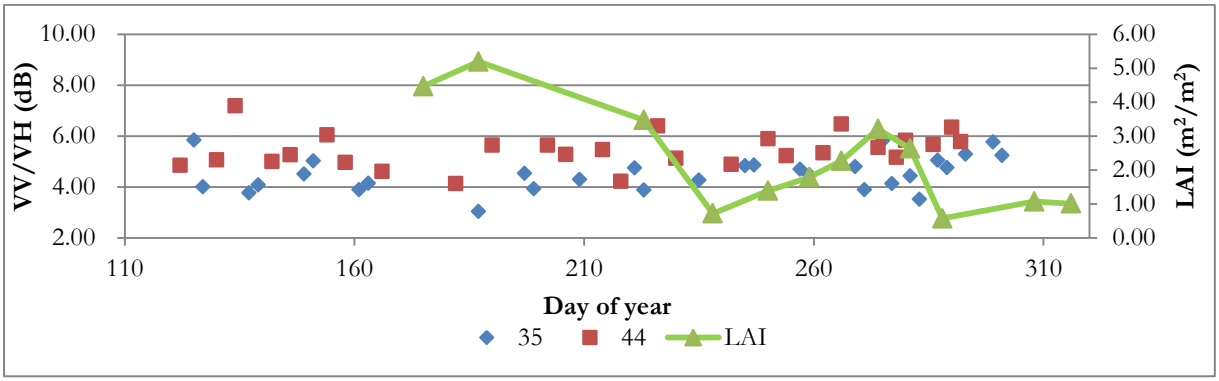

Figure 16 Time series of Sentinel-1 SAR backscatter coefficient in grass field (number 35, 44 means different incidence angles)

6.1.2. Spatial variation

In Figure 17, the all-time backscatter coefficient datasets are averaged for each measuring location in the field. Three corn fields (10-1, 7-1 and 7-3) are selected based on the complete dataset and intensive measurement. The horizontal axis shows the number of measuring location. The vertical axis shows the backscatter coefficient (VH, VV and VV/VH). These graphs show apparent variations of different locations in the field.

For corn field 10-1, location 1 and 2 have the highest average VH value as -17.62dB. The VH in location 5 is the lowest as -18.32dB. The highest VV value occurs in location 1 and 3 which is -11.24dB and the lowest is in location 5 which is -12.02dB. The highest VV/VH ratio value is in location 3 as 6.49dB and lowest value is in location 6 as 6.21dB. The difference between highest and lowest value of VH, VV and VV/VH are respectively 0.7, 0.78 and 0.28dB. The spatial variations in field 10-1 are not very distinct. Vegetation height and health condition are better in location 1, 2 and 3 than in 5.

For corn field 7-1, location 1 has the highest average VH value as -16.67dB. The VH in location 5 is the lowest as -17.92dB. The highest VV value occurs in location 2 which is -10.31dB and the lowest is in location 5 which is -11.91dB. The highest VV/VH ratio value is in location 2 as 7.05dB and lowest value is in location 4 as 5.89dB. The difference between highest and lowest value of VH, VV and VV/VH are respectively 1.25, 1.6 and 1.16dB. VV has the most obvious differences. The spatial variations in field 7-1 are more distinct than field 10-1. Vegetation height and health condition are better in location 1and 2 than in 5.

For corn field 7-3, location 1 has the highest average VH value as -15.51dB. The VH in location 3 is the lowest as -17.34dB. The highest VV value occurs in location 1 which is -9.42dB and the lowest is in location 3 which is -11.08dB. The highest VV/VH ratio value is in location 5 as 6.47dB and lowest value is in location 6 as 6.02dB. The difference between highest and lowest value of VH, VV and VV/VH are respectively 1.83, 1.66 and 0.45dB. The spatial variations in field 7-3 are more distinct than field 10-1 and 7-1. Vegetation height and health condition are better in location 1 than in 3.

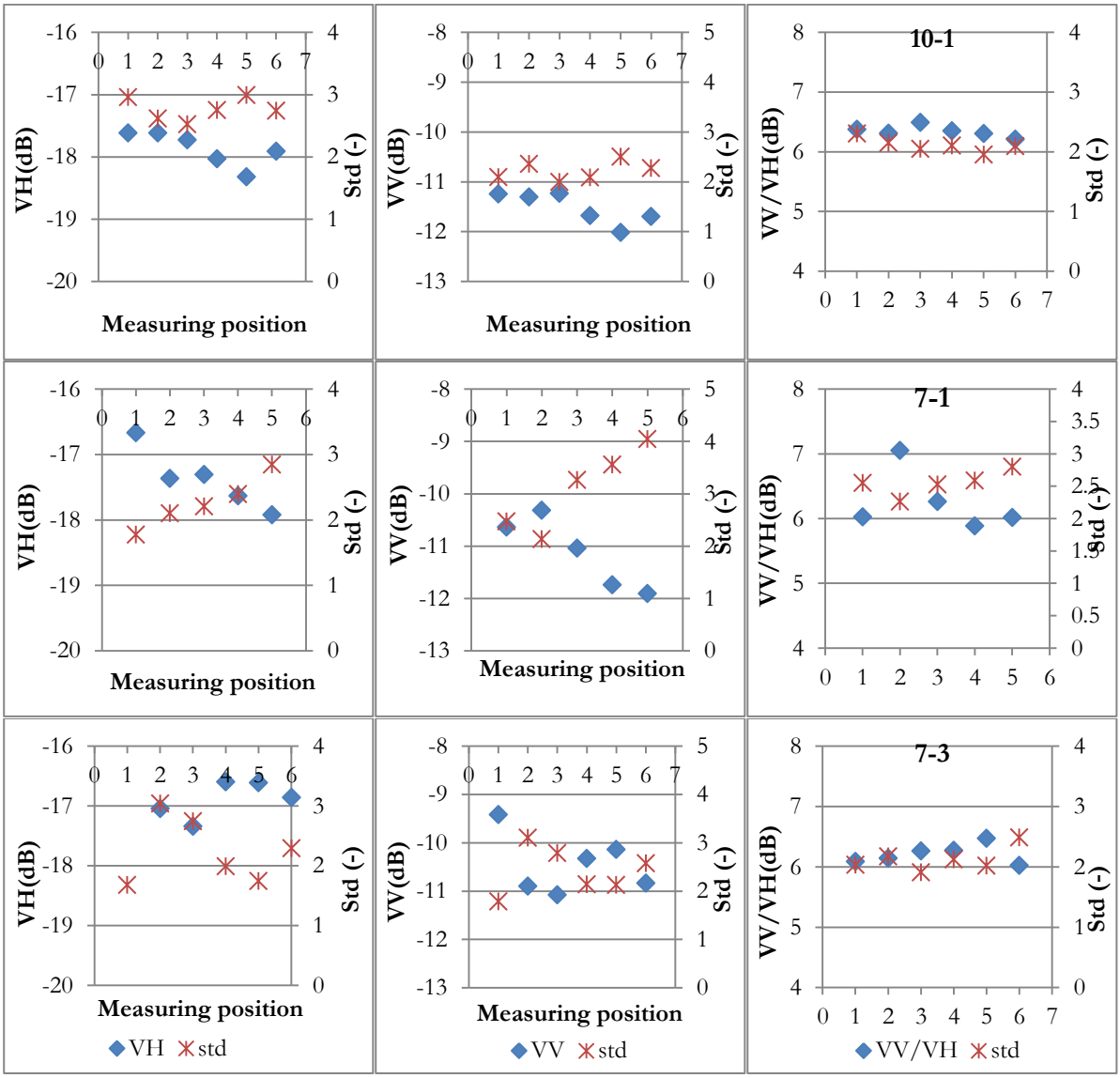

Figure 17 Spatial variability of backscatter coefficient in three corn fields

6.2. Correlations with LAI

To analyse the relationship between Sentinel-1 SAR and LAI measured in-situ, a correlation analysis was performed for all study fields. In Figure 18 and 18, dual-polarization ratio $\sigma^0_{VV}/\sigma^0_{VH}$ was plotted against LAI in each field. Figure 18 shows the normalized Sentinel-1 SAR data averaged over a size of 5 * 5 pixels centred on each measurement location against the LAI measured at these locations within four corn fields (field 10-1, 7-1, 7-3 and 2-2), one potato field(10-2) and one grass field(2-1). Figure 19 shows the correlation of normalized Sentinel-1 SAR and field averaged LAI. The exponential trend line and coefficient of determination R^2 are displayed as an indication for the found relationship.

From Figure 18, the correlation between point average polarization ratio and LAI is very low, the R^2 is not higher than 0.1. The LAI in field 7-1, 2-2 and 2-1 is negatively correlated with $\sigma^0_{VV}/\sigma^0_{VH}$ ratio. Referring to the research of Della Vecchia et al (2008), $\sigma^0_{VV}/\sigma^0_{VH}$ is negatively related with LAI in corn field. However, in field 10-2, 7-3 and 2-2, the $\sigma^0_{VV}/\sigma^0_{VH}$ ratio increased as LAI increase.

From Figure 19 appears that, the correlation between field average $\sigma^0_{VV}/\sigma^0_{VH}$ ratio and LAI is higher than the correlation at points. The LAI in field 7-1, 10-2 and 2-1 is negatively correlated with $\sigma^0_{VV}/\sigma^0_{VH}$ ratio. However, in field 10-1, 7-3 and 2-2, the $\sigma^0_{VV}/\sigma^0_{VH}$ ratio increased as LAI increased which is also not corresponding with the results from other literatures as mentioned above. The highest R^2 square value is 0.39 which happens in field 10-2. Field 7-1, 2-2 and 2-1 also have relatively higher correlations, the R^2 value ranges from 0.22 – 0.33. Correlation in field 10-1 and 7-3 are still not strong at all.

In general, the correlation between Sentinel-1 SAR dual-polarization ratio and LAI is weak. The correlation analysis shows different performance in these two methods. The field average data seems to be more correlated than the measuring location average data. This may be caused by the exaggerated noise from the combination of single data noise. So Sentinel-1 SAR is not a very good choice for exact LAI estimate, because the signals are small and the noise is fairly large.

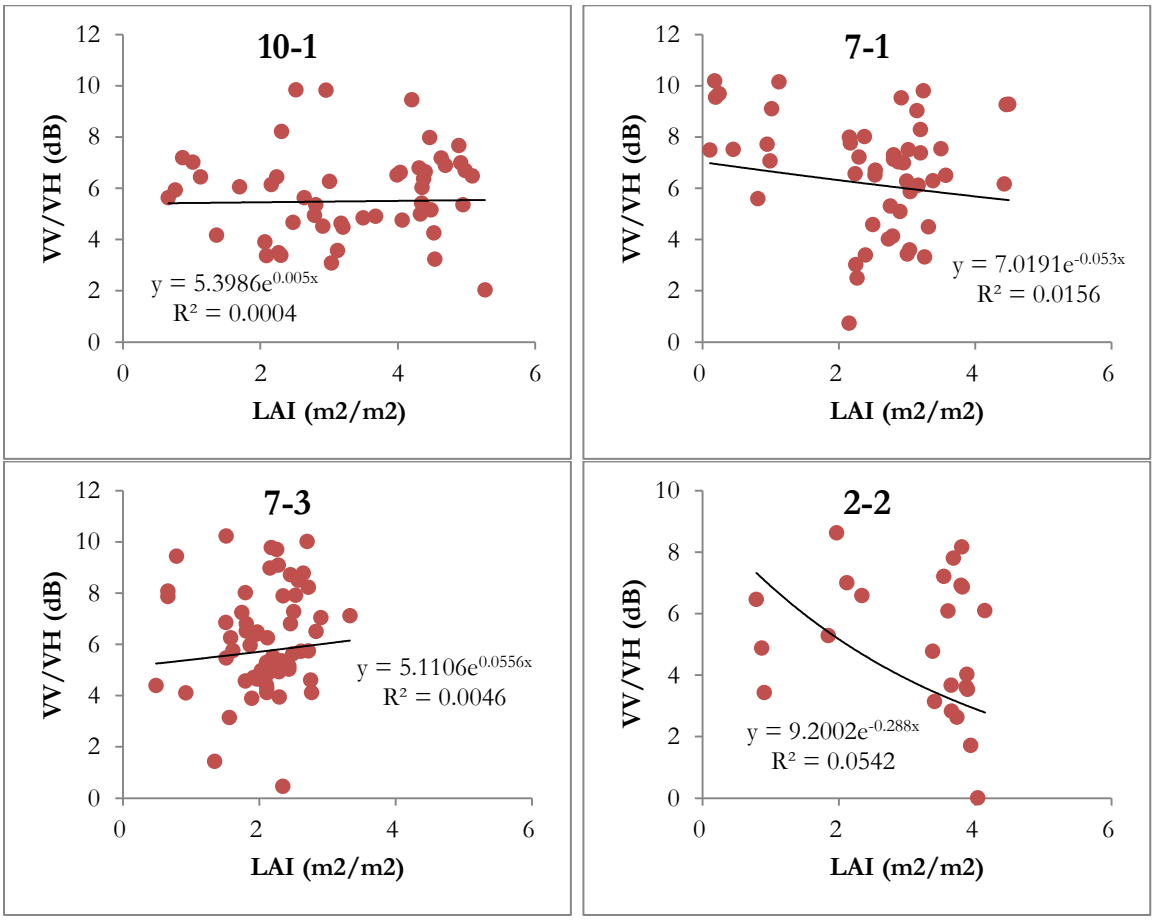

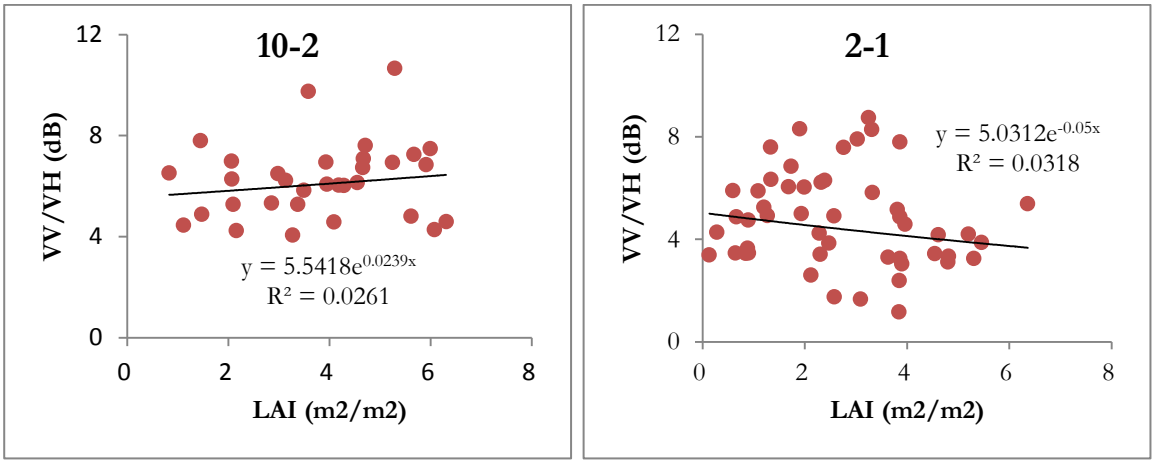

Figure 18 Correlation between dual polarization ratio $\sigma^0_{VV}/\sigma^0_{VH}$ for Sentinel-1 SAR and LAI measured in-situ for all the study fields (measuring position average)

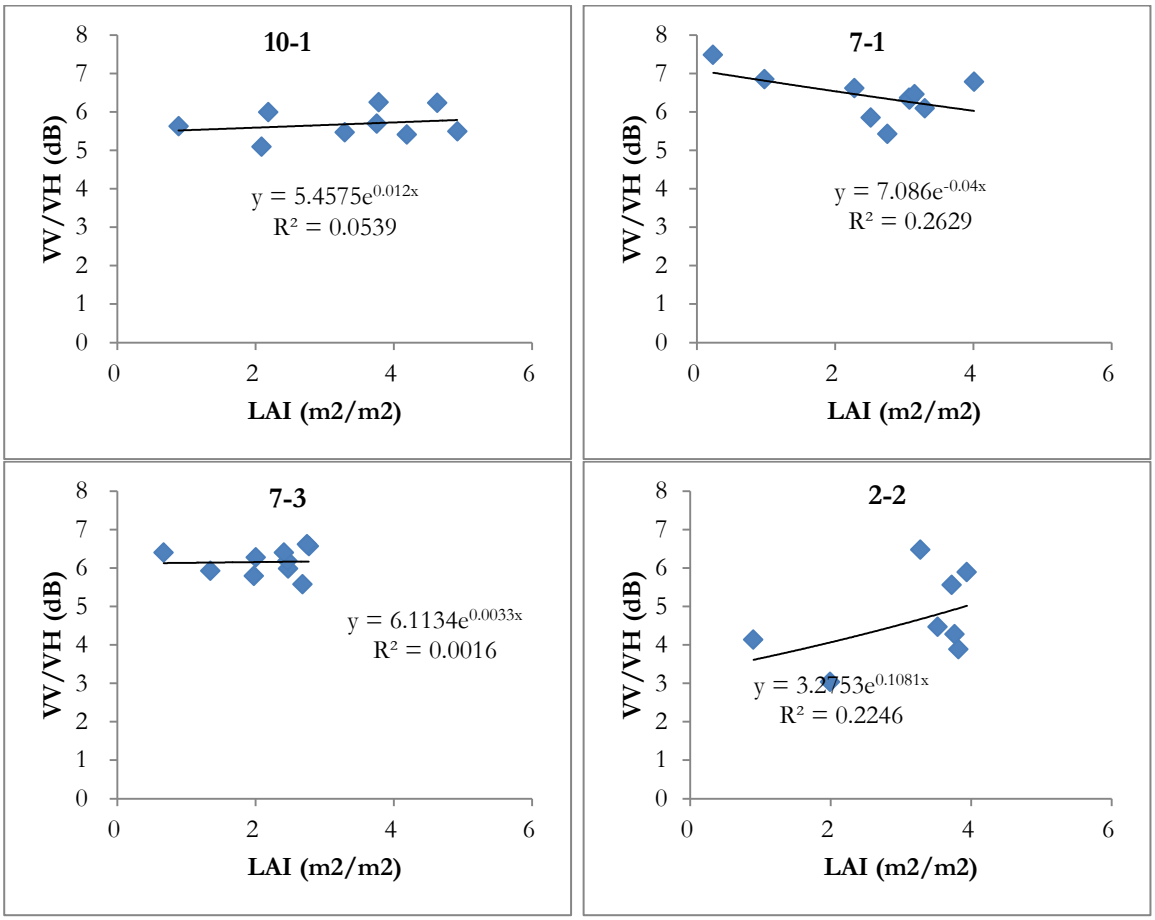

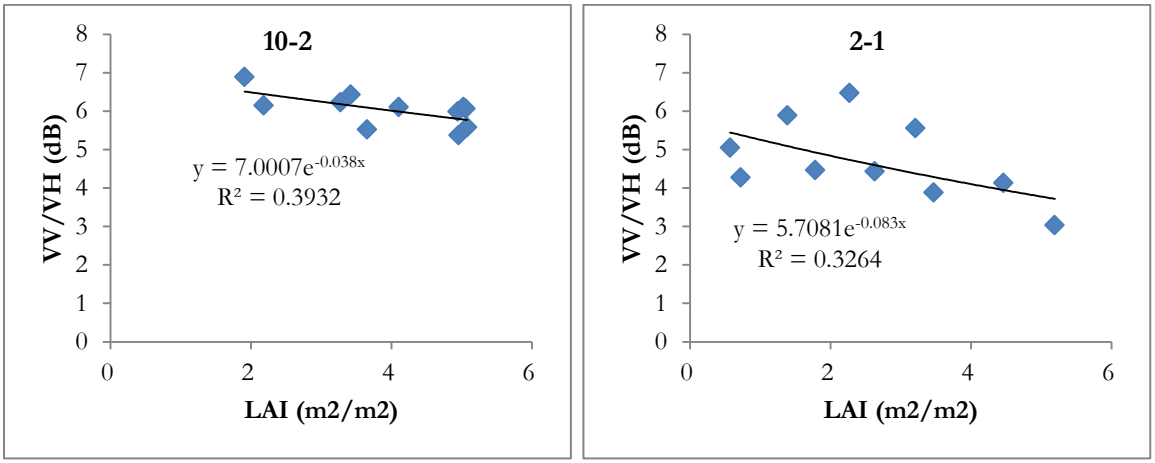

Figure 19 Correlation between dual polarization ratio $\sigma^0_{VV}/\sigma^0_{VH}$ for Sentinel-1 SAR and LAI measured in-situ for all the study fields (field average)

6.3. Backscatter coeffcient map in regional scale

Figure 20 shows the multi-temporal backscatter coefficient maps including σ^0_{VH}, σ^0_{VV} at the regional scale covering site 2 and site 7. The dual-polarization ratio $\sigma^0_{VV}/\sigma^0_{VH}$ maps were also plotted, but the variation is not very obvious which are displayed in the Appendix at the end of this thesis. The extent of this region is approximately 1890.5 hectare. The longitude and latitude of the map extent are respectively 52° 19' 33" N to 52° 24' 44" N and 6° 50' 31" E to 7° 01' 02" E. Eight maps are displayed from May to October which is the mainly grow stage for crops. The time interval between two maps is approximately 20-30 days.

For σ^0_{VH} maps, from May 13 to August 10, the signal σ^0_{VH} kept increasing for most of the area. This might indicate that the vegetation kept growing during this period and reached fully grown stage in August. From then until October 16, the σ^0_{VH} decreased. This may be the result of the wilting of vegetation and harvesting. However on July 24 and August 29, the VH is relatively lower than the reasonable trend. This may be caused by high frequency and high amount of rainfall events during this period. The impact of soil moisture on the backscatter coefficient increased.

For σ^0_{VV} maps, the globally temporal variation is not as obvious as σ^0_{VH}. From May 16 to August 10, a slightly increase of the signal σ^0_{VV} can be observed. Also from then until October 16, the σ^0_{VV} decreased slightly. On the other hand, considering both the σ^0_{VV} and σ^0_{VH} maps of the same date and the investigation of real field condition, three are three areas located in the center, right and bottom of the map respectively, have high σ^0_{VV} and σ^0_{VH} at the same time. These areas are residential area. the is good for distinguishing the land cover and land use. Comparing with signal σ^0_{VH}, σ^0_{VV} is more sensitive to non-vegetation area like buildings and bare lands as can be seen from maps on July 24 and August 29.

The conclusion is that σ^0_{VH} is the most sensitive parameter among these three to show the global temporal variation of vegetation growth at a relatively large scale. σ^0_{VV} is not that sensitive to tell the vegetation grow stage in the map. However considering both σ^0_{VV} and σ^0_{VH} in the research is suitable for distinguish vegetated and non-vegetated area.

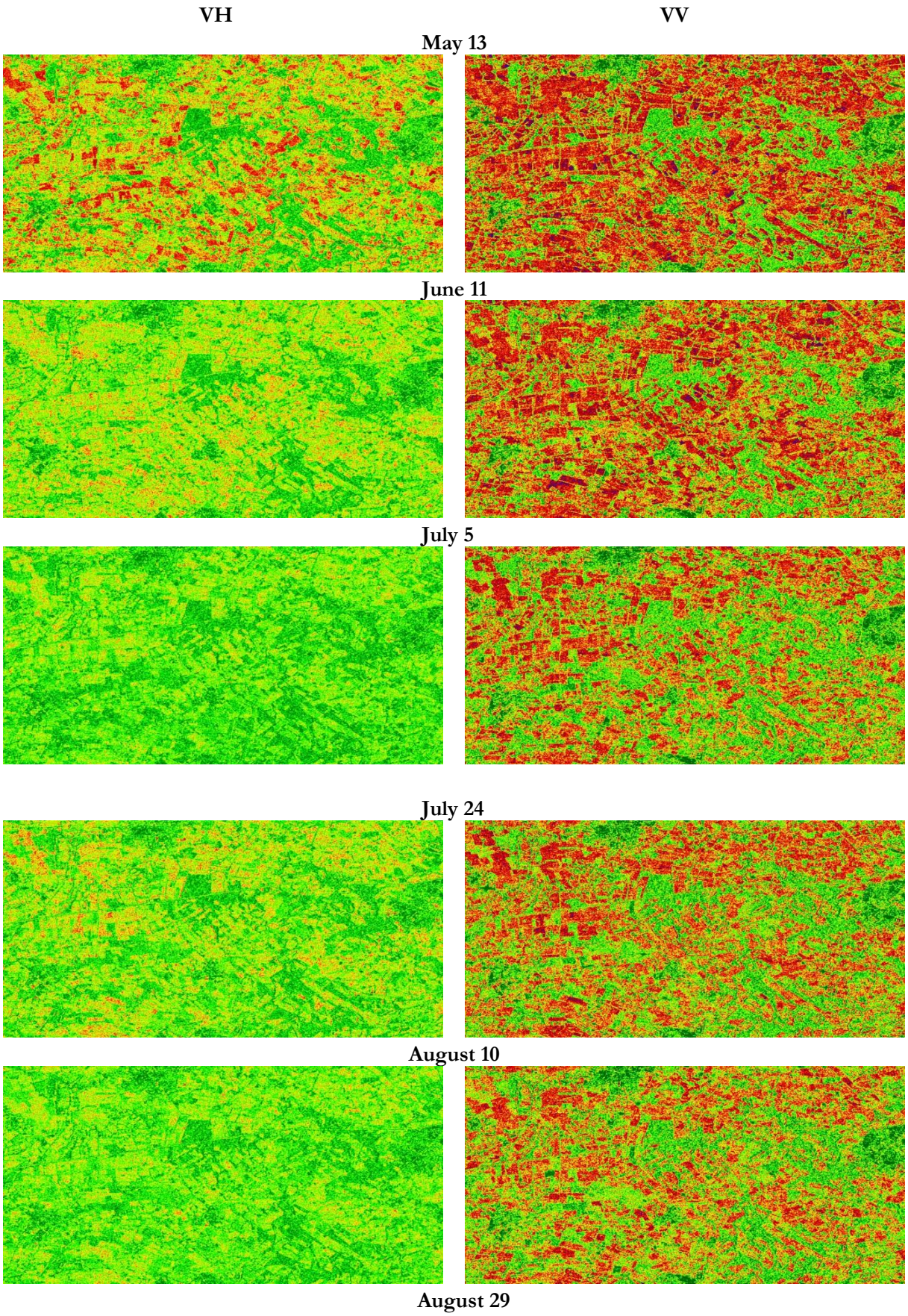
VH
VV
May 13
June 11
July 5
July 24
August 10
August 29

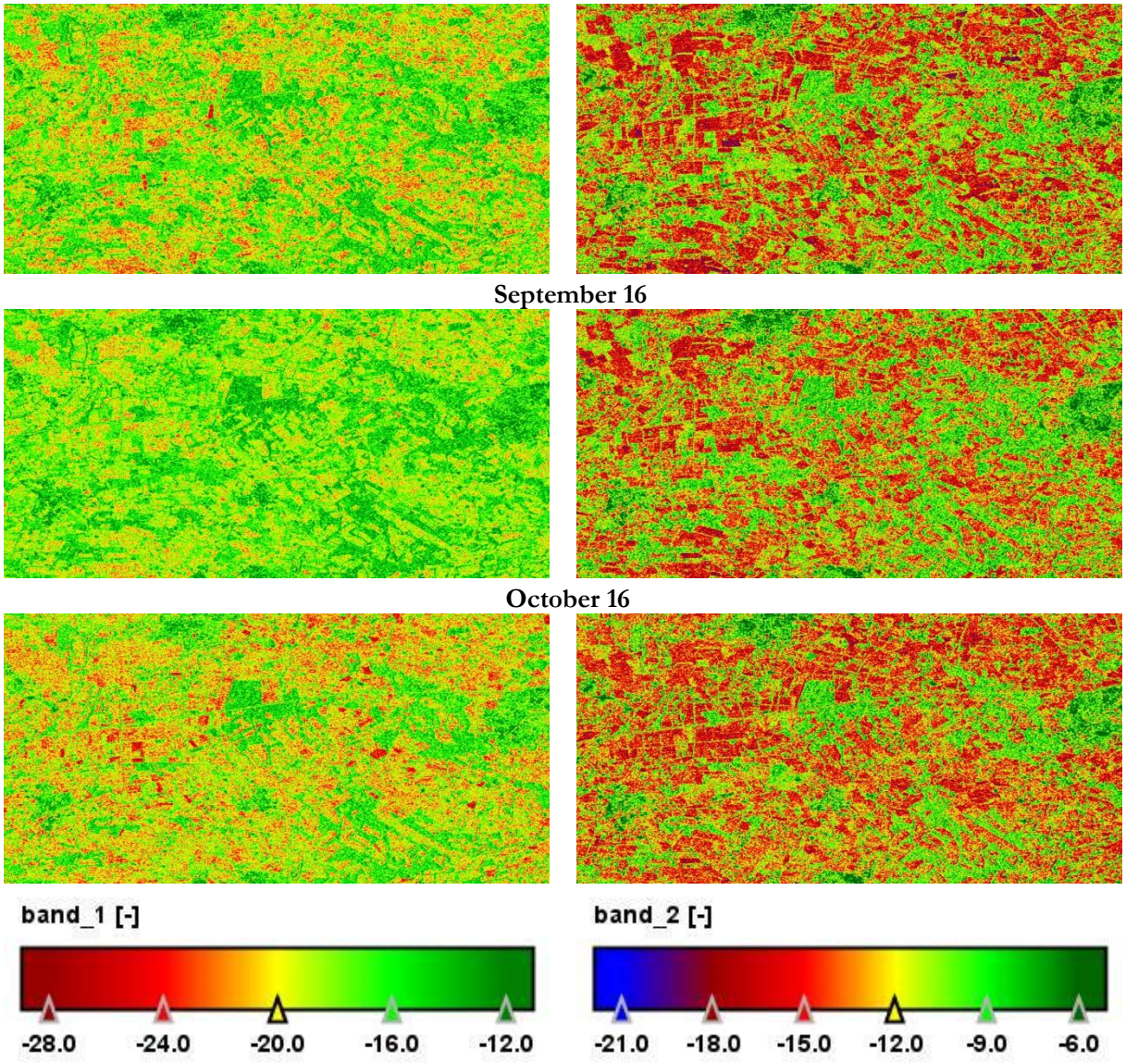

Figure 20 The multi-temporal maps of backscatter coefficient σ^0_{VV} and σ^0_{VH} in a region covering site 2 and site 7. The date of maps are indicated above the image.

7. SUMMARY AND CONCLUSIONS

For this study, the intensive measurements of vegetation variables (e.g. vegetation height and LAI) and rainfall interception collected in the Twente region from May to October in 2016 were analysed. The measurements were taken in six fields, four corn fields, one potato field and one grass field. The Sentinel-1 SAR data of the area was also processed to analyse its ability to distinguish vegetation growth and correlation with LAI.

How does the interception by vegetation vary spatially and temporally in year 2016?
For field 10-1, while the plants are fully grown, the ratio remains at a low level around 0.1 - 0.2 which indicates that quite a lot of water being intercepted. After that. While the plants were in senescence stage, the ratio increases slightly. For field 7-3, the ratio also decreases as the corn plants grow. On DOY 302, the ratio is the lowest as 0.12.While the plants are fully grown, the ratio kept stable at a low level around 0.3 - 0.5. The interception of field 10-1 at fully grown stage is higher than that in field 7-3. The LAI of fields 10-1 is also higher than that in field 7-3 at fully grown stage. For the spatially variation, the bottle rain collectors are considered. The results from single bottle have a relatively large difference with rain gauge measurements. However, the average of all the locations has a well correspondence with rain gauge results. The results from bottles between the corn rows also have a relatively large difference with rain gauge measurements but the ones from bottles in the row have a better match.

Is the Sentinel-1 dual-polarization ratio sensitive enough for quantifying the LAI?
In general, the correlation between Sentinel-1 SAR dual-polarization ratio and LAI is weak. The correlation analysis shows different performance in location average and field average results. The field average data seems to be more correlated than the measuring location average data. For the location average data, the R^2 is not higher than 0.1. This may be caused by the exaggerated noise from the combination of single data noise. For field average data, fields 7-1, 2-2 and 2-1 have relatively increased correlations, the R^2 value ranges from 0.22 – 0.33. This improvement may because of the average over the field also average and reduce the single data noise, but the correlation is still not strong enough. So Sentinel-1 SAR is not a very good choice for exact LAI estimate, because the signals are small and the noise is fairly large.

Can Sentinel-1 backscatter observation be used to detect different vegetation growth stages?
The conclusion is that σ^0_{VH} is a more sensitive parameter than σ^0_{VV} and $\sigma^0_{VV}/\sigma^0_{VH}$ to show the global temporal variation of vegetation growth at a relatively large scale. σ^0_{VV} is not that sensitive to tell the vegetation grow stage in the map. However considering both σ^0_{VV} and σ^0_{VH} in the research is suitable for distinguish vegetated and non-vegetated area. But in the rainy season, the soil moisture kind of disturbs the influence of vegetation to backscatter, so it is hard to detect vegetation growth stages under this condition.

Is the LAI a vegetation variable with which the rainfall interception can be estimated reliably?
The results show that there exists a positive correlation between LAI and rainfall interception. But it is hard to quantify interception only with LAI.

8. RECOMMENDATION

Considering the result from spatial variation of LAI and interception, the spatial variability is large enough for more locations induced to the measurements which accounts for 30% to 40% of the average value. in the future study, more points for vegetation variable, rainfall and throughfall in-situ measurements should be concluded.

Many uncertainties may happen during the measurements. There are some very tall walnut trees near the fields 7-1 and 7-3. The shade of tree will influence the signal received by the sensor of LAI – 2000 instruments. In potato field 10-2, the plants are densely distributed and the under canopy readings of LAI measurement are difficult to get. All these uncertainties may lead to the errors for LAI measurements. The recommendation for the future is taking care of these conditions while applying LAI measurement.

This study only performed measurements in one growing season. Due to the variations in weather, temperature, rainfall and soil condition etc. for different growing seasons, the single growing season measurement may not be representative enough to the normal condition. So next time, the continuously measurements of multiple growing seasons may be needed.

The effect of soil moisture on SAR backscatter isn't considered in this study. Soil moisture is reported to also have influence on the backscatter (Gherboudj, Magagi, Berg, & Toth, 2011). especially from August to September, the rainfall happens a lot. The sudden soil moisture change may also impact the pattern of backscatter. So in the future study better taking consideration of soil moisture measurements as well.

LIST OF REFERENCES

Attema, E. P. W., & Ulaby, F. T. (1978). Vegetation modeled as a water cloud. *Radio Science*, *13*(2), 357–364. http://doi.org/10.1029/RS013i002p00357

Baghdadi, N., Boyer, N., Todoroff, P., El Hajj, M., & B??gu??, A. (2009). Potential of SAR sensors TerraSAR-X, ASAR/ENVISAT and PALSAR/ALOS for monitoring sugarcane crops on Reunion Island. *Remote Sensing of Environment*, *113*(8), 1724–1738. http://doi.org/10.1016/j.rse.2009.04.005

Bakar, S. B. A., Shaari, A. T., Chuah, H. T., & Ewe, H. T. (1997). A preliminary study of phenological growth stages of wetland rice using ERS1/2 SAR data. *Geoscience and Remote Sensing, 1997. IGARSS '97. Remote Sensing - A Scientific Vision for Sustainable Development., 1997 IEEE International*, *2*(d), 1069–1071 vol.2. http://doi.org/10.1109/IGARSS.1997.615345

Bauer, J., Siegmann, B., Jarmer, T., & Aschenbruck, N. (2016). On the potential of Wireless Sensor Networks for the in-situ assessment of crop leaf area index. *Computers and Electronics in Agriculture*, *128*, 149–159. http://doi.org/10.1016/j.compag.2016.08.019

Bracaglia, M., Ferrazzoli, P., & Guerriero, L. (1995). A fully polarimetric multiple scattering model for crops. *Remote Sensing of Environment*, *54*(3), 170–179. http://doi.org/10.1016/0034-4257(95)00151-4

Brandão, Z. N., & Zonta, J. H. (2016). Hemispherical photography to estimate biophysical variables of cotton. *Revista Brasileira de Engenharia Agrícola E Ambiental*, 789–794.

Carlyle-Moses, D. E., & Price, A. G. (1999). An evaluation of the Gash interception model in a northern hardwood stand. *Journal of Hydrology*, *214*(1–4), 103–110. http://doi.org/10.1016/S0022-1694(98)00274-1

Chen, J. M., Pavlic, G., Brown, L., Cihlar, J., Leblanc, S. G., White, H. P., … Pellikka, P. K. E. (2002). Derivation and validation of Canada-wide coarse-resolution leaf area index maps using high-resolution satellite imagery and ground measurements. *Remote Sensing of Environment*, *80*, 165–184.

Colombo, R., Bellingeri, D., Fasolini, D., & Marino, C. M. (2003). Retrieval of leaf area index in different vegetation types using high resolution satellite data. *Remote Sensing of Environment*, *86*, 120–131. http://doi.org/10.1016/S0034-4257(03)00094-4

Cookmartin, G., Saich, P., Quegan, S., Cordey, R., Burgess-Alien, P., & Sowter, A. (2000). Modeling microwave interactions with crops and comparison with ERS2 SAR observations. *IEEE Transactions on Geoscience and Remote Sensing*, *38*(2 I), 658–670. http://doi.org/10.1109/36.841996

Crockford, R. H., & Richardson, D. P. (2000). Partitioning of rainfall into throughfall, stemflow and interception:effect of forest type, ground cover and climate. *Hydrological Processes*, *14*(April 1999), 2903–2920.

Cuartas, L. A., Tomasella, J., Nobre, A. D., Hodnett, M. G., Waterloo, M. J., & Múnera, J. C. (2007). Interception water-partitioning dynamics for a pristine rainforest in Central Amazonia: Marked differences between normal and dry years. *Agricultural and Forest Meteorology*, *145*(1–2), 69–83. http://doi.org/10.1016/j.agrformet.2007.04.008

Czikowsky, M. J., & Fitzjarrald, D. R. (2009). Detecting rainfall interception in an Amazonian rain forest with eddy flux measurements. *Journal of Hydrology*, *377*(1–2), 92–105. http://doi.org/10.1016/j.jhydrol.2009.08.002

Della Vecchia, A., Ferrazzoli, P., Guerriero, L., Ninivaggi, L., Strozzi, T., & Wegm??ller, U. (2008). Observing and modeling multifrequency scattering of maize during the whole growth cycle. *IEEE Transactions on Geoscience and Remote Sensing*, *46*(11), 3709–3718. http://doi.org/10.1109/TGRS.2008.2001885

Frasson, R. P. de M., & Krajewski, W. F. (2013). Rainfall interception by maize canopy: Development and application of a process-based model. *Journal of Hydrology*, *489*, 246–255. http://doi.org/10.1016/j.jhydrol.2013.03.019

FRIEDL, M. A., MICHAELSEN, J., DAVIS, F. W., WALKER, H., & SCHIMEL, D. S. (1994). Estimating grassland biomass and leaf area index using ground and satellite data. *International Journal of Remote Sensing*, *15*(7), 1401–1420. Retrieved from http://cat.inist.fr/?aModele=afficheN&cpsidt=4151946

Gagnon, L., & Jouan, A. (1997). Speckle filtering of SAR images: a comparative study between complex-wavelet-based and standard filters. *Proceedings of SPIE*, *3169*, 80–91. http://doi.org/10.1117/12.279681

Gash, J. H. C. (1979). An analytical model of rainfall interception by forests. *Quarterly Journal of the Royal Meteorological Society*, *105*(443), 43–55. http://doi.org/10.1002/qj.49710544304

Gash, J. H. C., Lloyd, C. R., & Lachaud, G. (1995). Estimating sparse forest rainfall interception with an analytical model. *Journal of Hydrology*, *170*(1–4), 79–86. http://doi.org/10.1016/0022-1694(95)02697-N

Gerrits, A. M. J., Pfister, L., & Savenije, H. H. G. (2010). Spatial and temporal variability of canopy and forest floor interception in a beech forest. *Hydrological Processes1. Gerrits, A. M. J., Pfister, L. & Savenije, H. H. G. Spatial and Temporal Variability of Canopy and Forest Floor Interception in a Beech Forest. Hydrol. Process. 24, 3011–3025 (2010).*, *24*(21), 3011–3025. http://doi.org/10.1002/hyp.7712

Gherboudj, I., Magagi, R., Berg, A. A., & Toth, B. (2011). Soil moisture retrieval over agricultural fields from multi-polarized and multi-angular RADARSAT-2 SAR data. *Remote Sensing of Environment*, *115*(1), 33–43. http://doi.org/10.1016/j.rse.2010.07.011

Gomez-Peralta, D., Oberbauer, S. F., McClain, M. E., & Philippi, T. E. (2008). Rainfall and cloud-water interception in tropical montane forests in the eastern Andes of Central Peru. *Forest Ecology and Management*, *255*(3–4), 1315–1325. http://doi.org/10.1016/j.foreco.2007.10.058

Hosseini, M., McNairn, H., Merzouki, A., & Pacheco, A. (2015). Estimation of Leaf Area Index (LAI) in corn and soybeans using multi-polarization C- and L-band radar data. *Remote Sensing of Environment*, *170*, 77–89. http://doi.org/10.1016/j.rse.2015.09.002

Jackson, N. A. (2000). Measured and modelled rainfall interception loss from an agroforestry system in Kenya. *Agricultural and Forest Meteorology*, *100*(4), 323–336. http://doi.org/10.1016/S0168-1923(99)00145-8

Jiao, X., McNairn, H., Shang, J., Pattey, E., Liu, J., & Champagne, C. (2011). The sensitivity of RADARSAT-2 polarimetric SAR data to corn and soybean leaf area index. *Canadian Journal of Remote Sensing*, *37*(1), 69–81. http://doi.org/10.5589/m11-023

Kozak, J. A., Ahuja, L. R., Green, T. R., & Ma, L. (2007). Modelling crop canopy and residue rainfall interception effects on soil hydrological components for semi-arid agriculture. *Hydrological Processes*, *21*(2), 229–241. http://doi.org/10.1002/hyp.6235

Leuning, R., Condon, A. G., Dunin, F. X., Zegelin, S., & Denmead, O. T. (1994). Rainfall interception and evaporation from soil below a wheat canopy. *Agricultural and Forest Meteorology*, *67*(3–4), 221–238. http://doi.org/10.1016/0168-1923(94)90004-3

Limousin, J. M., Rambal, S., Ourcival, J. M., & Joffre, R. (2008). Modelling rainfall interception in a mediterranean Quercus ilex ecosystem: Lesson from a throughfall exclusion experiment. *Journal of Hydrology*, *357*(1–2), 57–66. http://doi.org/10.1016/j.jhydrol.2008.05.001

Lin, H., Chen, J., Pei, Z., Zhang, S., & Hu, X. (2009). Monitoring sugarcane growth using ENVISAT ASAR data. *IEEE Transactions on Geoscience and Remote Sensing*, *47*(8), 2572–2580. http://doi.org/10.1109/TGRS.2009.2015769

LIU Zhangwen, 刘章文, CHEN Rensheng, 陈仁升, SONG Yaoxuan, 宋耀选, & HAN Chuntan, 韩春坛. (2012). Characteristics of rainfall interception for four typical shrubs in Qilian Mountain. *Acta Ecologica Sinica*, *32*(4), 1337–1346. http://doi.org/10.5846/stxb201012211822

Merriam, R. A. (1960). A note on the interception loss equation. *Journal of Geophysical Research*, *65*(11), 3850–3851. http://doi.org/10.1029/JZ065i011p03850

Motahari, M., Attarod, P., Pypker, T. G., Etemad, V., & Shirvany, A. (2013). Rainfall interception in a Pinus eldarica plantation in a semiarid climate zone: An application of the gash model. *Journal of Agricultural Science and Technology*, *15*(5), 981–994.

Muzylo, A., Llorens, P., Valente, F., Keizer, J. J., Domingo, F., & Gash, J. H. C. (2009). A review of rainfall interception modelling. *Journal of Hydrology*, *370*(1–4), 191–206. http://doi.org/10.1016/j.jhydrol.2009.02.058

Myneni, R. B., Nemani, R. R., & Running, S. W. (1997). Estimation of Global Leaf Area Index and Absorbed Par Using Radiative Transfer Models. *IEEE TRANSACTIONS ON GEOSCIENCE AND REMOTE SENSING*, *35*(6), 1380–1393.

Pearse, G. D., Watt, M. S., & Morgenroth, J. (2016). Comparison of optical LAI measurements under diffuse and clear skies after correcting for scattered radiation. *Agricultural and Forest Meteorology*, *221*, 61–70. http://doi.org/10.1016/j.agrformet.2016.02.001

Rutter, A. J., Kershaw, K. A., Robins, P. C., & Morton, A. J. (1971). A predictive model of rainfall interception in forests, 1. Derivation of the model from observations in a plantation of Corsican pine. *Agricultural Meteorology*, *9*, 367–384. http://doi.org/http://dx.doi.org/10.1016/0002-1571(71)90034-3

Su, L., Zhao, C., Xu, W., & Xie, Z. (2016). Modeling interception loss using the revised Gash model: a case study in a mixed evergreen and deciduous broadleaved forest in China. *Ecohydrology*. http://doi.org/10.1002/eco.1749

Torres, R., Snoeij, P., Geudtner, D., Bibby, D., Davidson, M., Attema, E., … Rostan, F. (2012). GMES Sentinel-1 mission. *Remote Sensing of Environment*, *120*, 9–24. http://doi.org/10.1016/j.rse.2011.05.028

van Dijk, A. I. J. ., & Bruijnzeel, L. . (2001). Modelling rainfall interception by vegetation of variable density using an adapted analytical model. Part 1. Model description. *Journal of Hydrology*, *247*(3–4), 230–238. http://doi.org/10.1016/S0022-1694(01)00392-4

Van Dijk, A. I. J. M., & Bruijnzeel, L. A. (2001). Modelling rainfall interception by vegetation of variable density using an adapted analytical model. Part 2. Model validation for a tropical upland mixed cropping system. *Journal of Hydrology*, *247*(3–4), 239–262. http://doi.org/10.1016/S0022-1694(01)00393-6

Vernimmen, R. R. E., Bruijnzeel, L. A., Romdoni, A., & Proctor, J. (2007). Rainfall interception in three contrasting lowland rain forest types in Central Kalimantan, Indonesia. *Journal of Hydrology*, *340*(3–4), 217–232. http://doi.org/10.1016/j.jhydrol.2007.04.009

Woodgate, W., Armston, J. D., Disney, M., Jones, S. D., Suarez, L., Hill, M. J., … Soto-berelov, M. (2016). Agricultural and Forest Meteorology Quantifying the impact of woody material on leaf area index estimation from hemispherical photography using 3D canopy simulations. *Agricultural and Forest Meteorology*, *226–227*, 1–12. http://doi.org/10.1016/j.agrformet.2016.05.009

Wösten, H., De Vries, F., Hoogland, T., Massop, H. T. L., Veldhuizen, A. A., Vroon, H., … Bolman, A. (2013). *BOFEK2012, de nieuwe, bodemfysische schematisatie van Nederland [BOFEK2012; the new soil physical schematization of the Netherlands, in Dutch]*. *Alterra report* (Vol. 2387). Retrieved from http://edepot.wur.nl/247678

APPENDIX

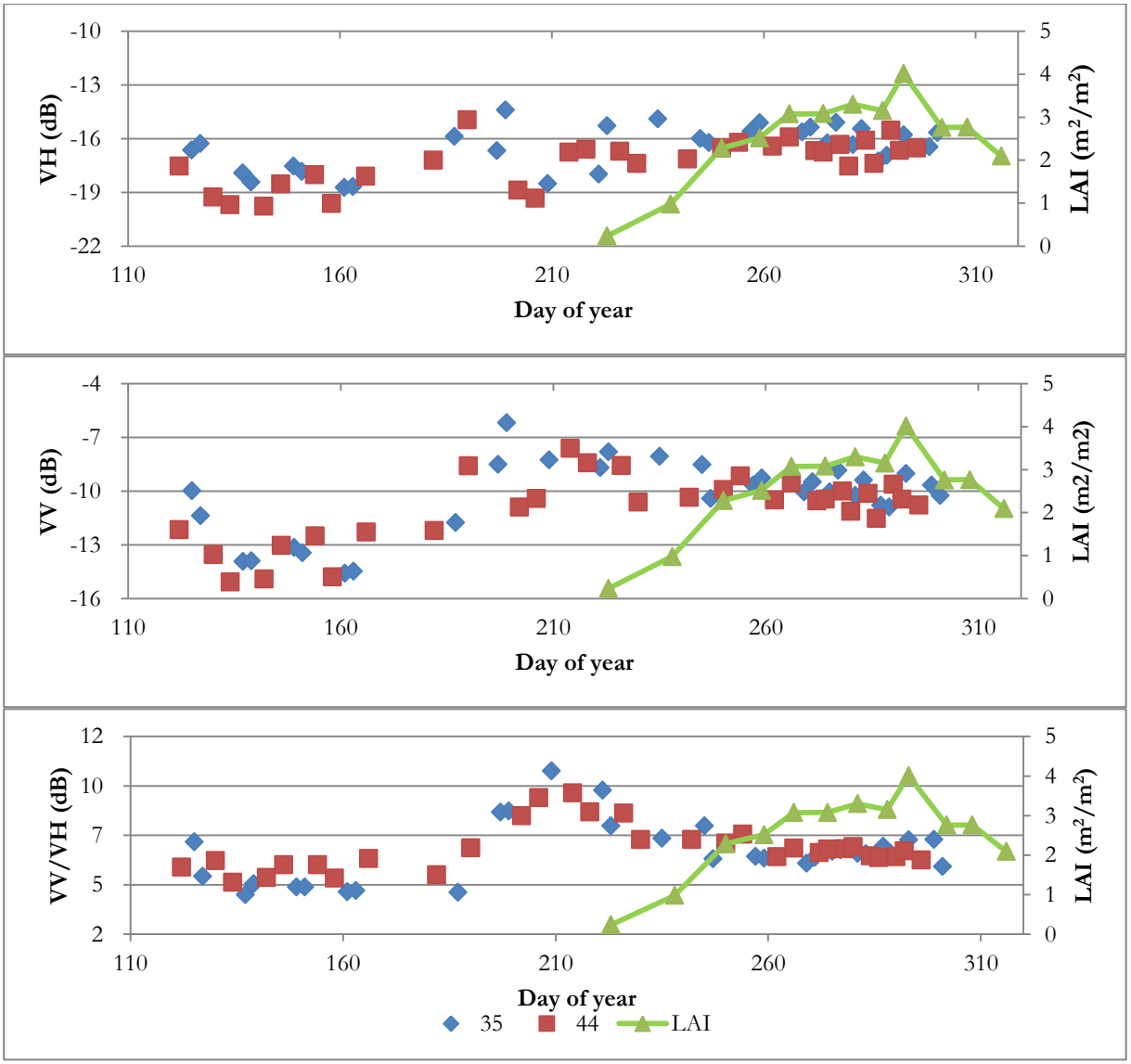

Figure 21 Time series of Sentinel-1 SAR backscatter coefficient in corn field 7-1

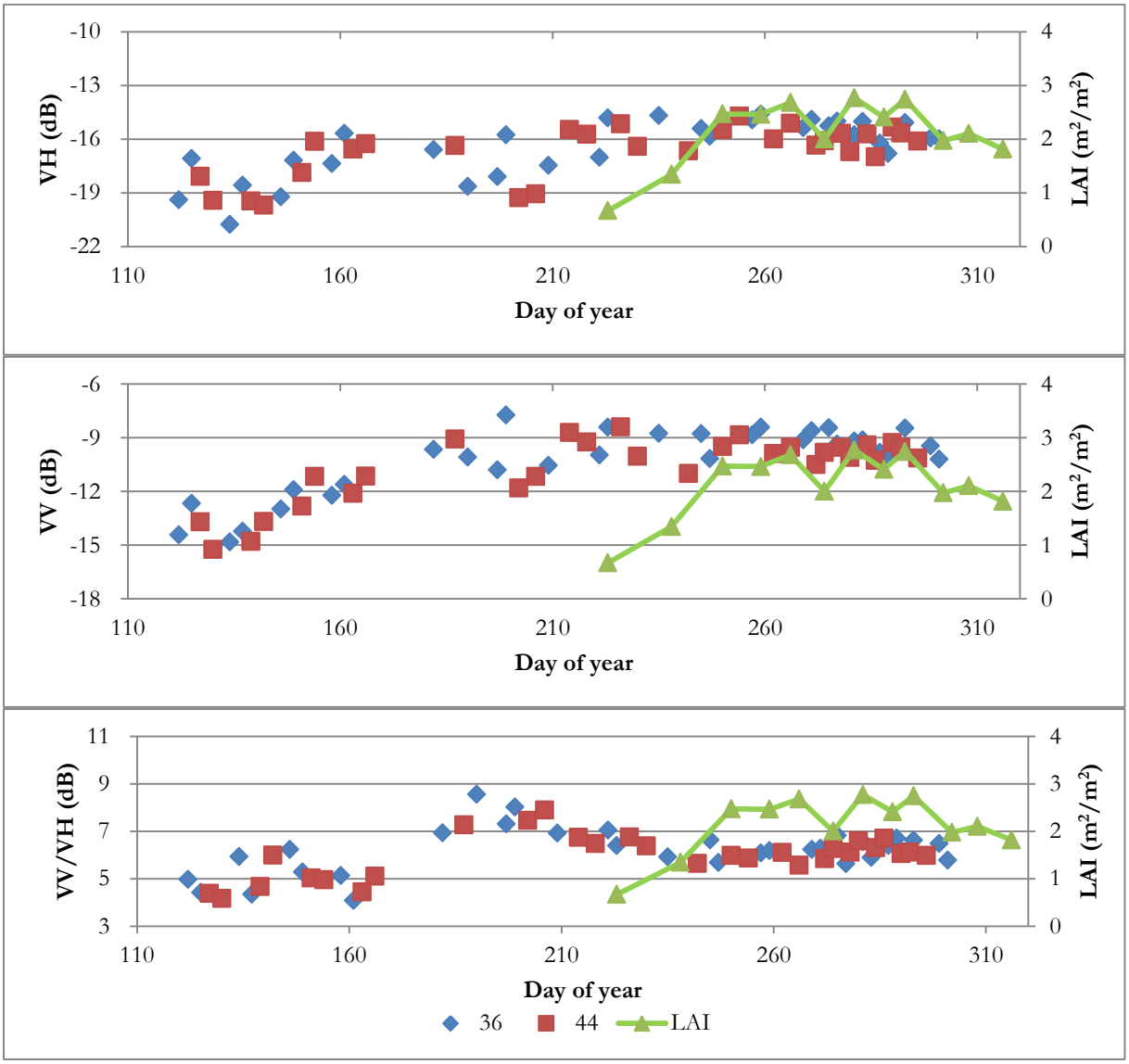

Figure 22 Time series of Sentinel-1 SAR backscatter coefficient in corn field 7-3

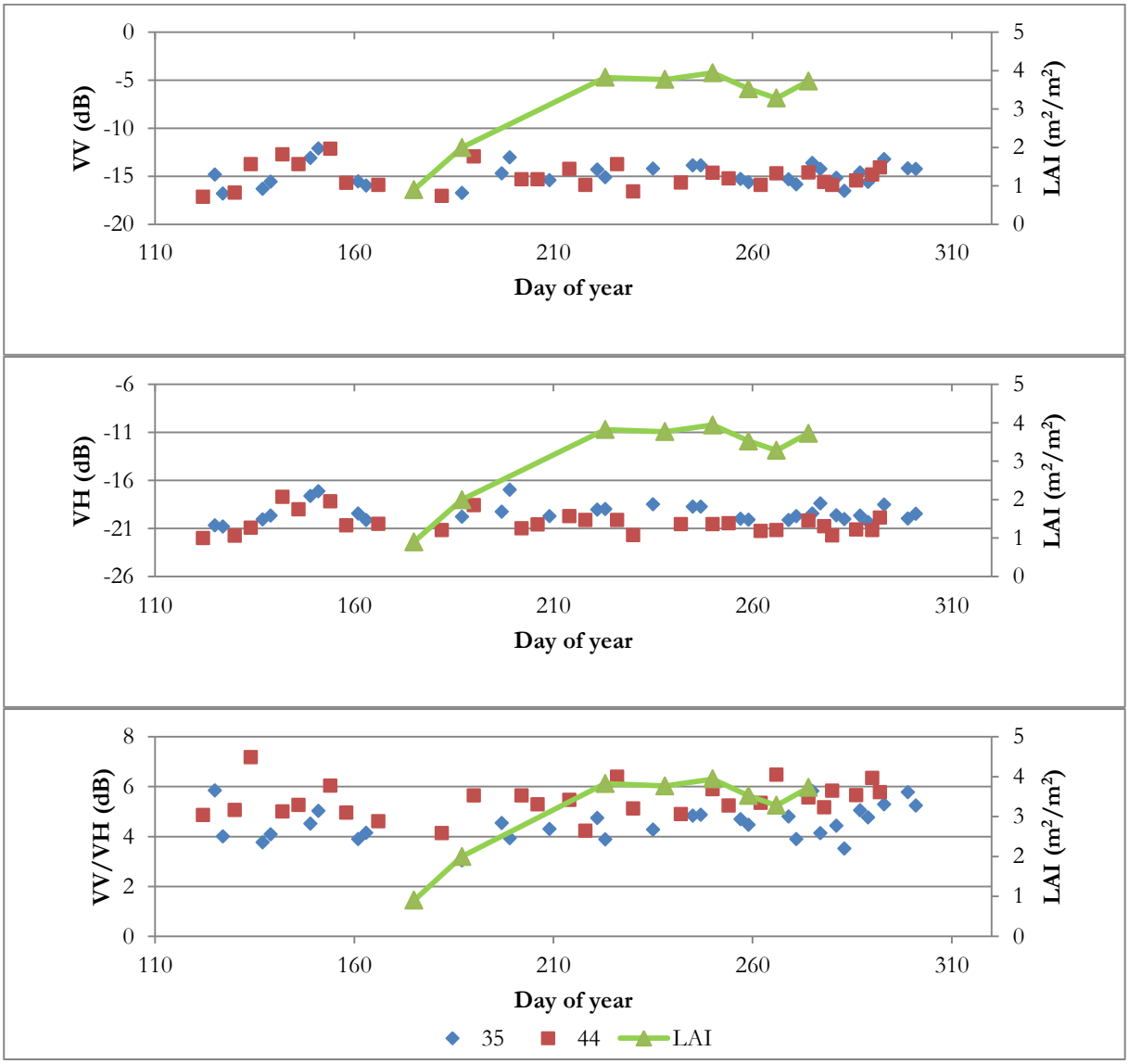

Figure 23 Time series of Sentinel-1 SAR backscatter coefficient in corn field 2-2

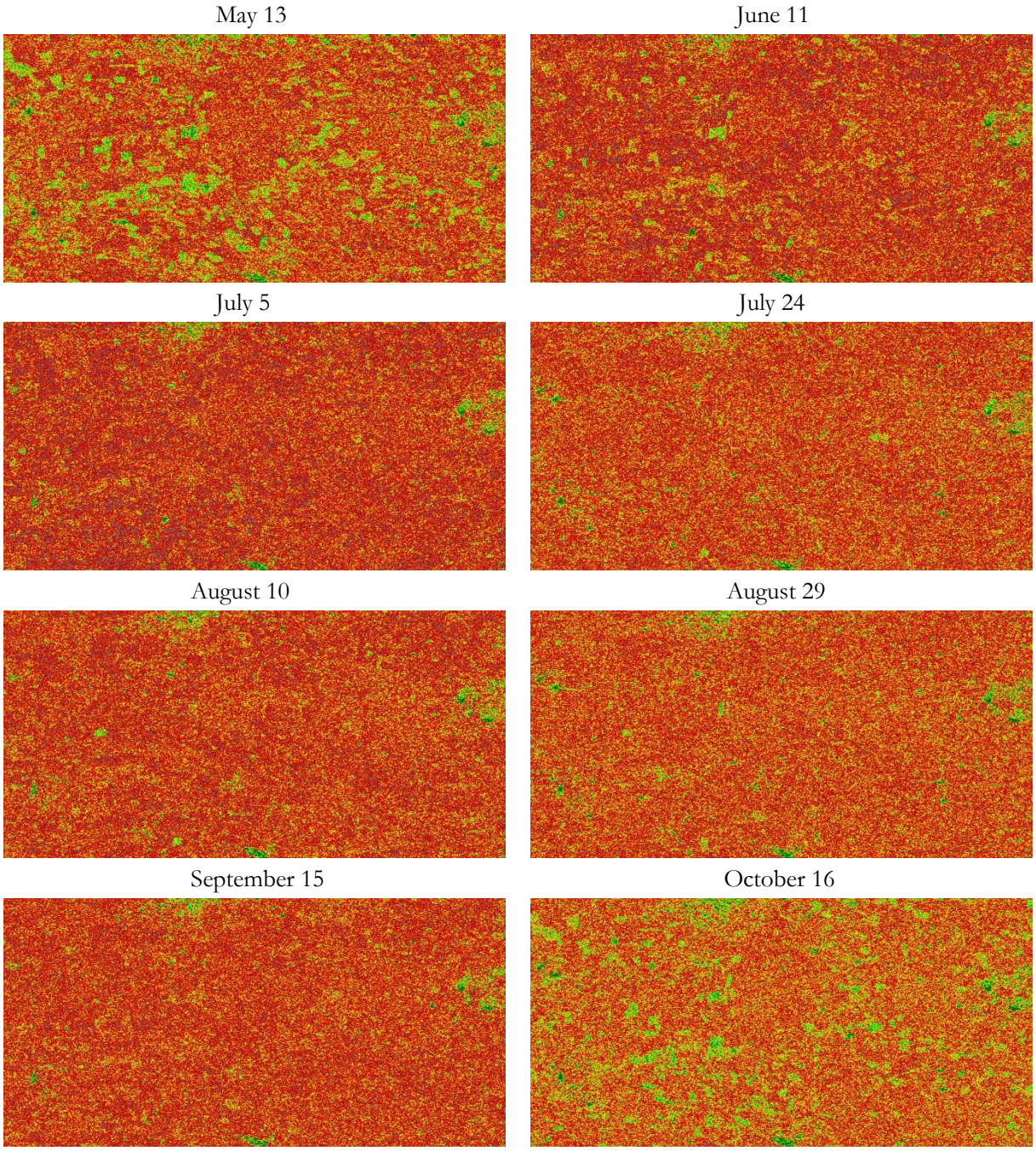

Figure 24 The multi-temporal maps of backscatter coefficient $\sigma^0_{VV}/\sigma^0_{VH}$ in a region covering site 2 and site 7. The date of maps are indicated above the image.